SANDIA REPORT

NUREG/CR–5120
SAND88-8213
R4
Printed May 1988

A Model for the Transport and Chemical Reaction of Molten Debris in Direct Containment Heating Experiments

K. D. Marx

Prepared by
Sandia National Laboratories
Albuquerque, New Mexico 87185 and Livermore, California 94550
for the United States Department of Energy
under Contract DE-AC04-76DP00789

Prepared for
U.S. NUCLEAR REGULATORY COMMISSION

Issued by Sandia National Laboratories, operated for the United States Department of Energy by Sandia Corporation.

NUREG/CR-5120
SAND88-8213
R4

A MODEL FOR THE TRANSPORT AND CHEMICAL REACTION OF MOLTEN DEBRIS IN DIRECT CONTAINMENT HEATING EXPERIMENTS

K. D. Marx

May 1988

Sandia National Laboratories
Livermore, CA 94550
Operated by
Sandia Corporation
for the
U. S. Department of Energy

Prepared for
Division of Reactor System Safety
Office of Nuclear Regulatory Research
U. S. Nuclear Regulatory Commission
Washington, DC 20555
Under Memorandum of Understanding DOE 40-550-75
NRC FIN Nos. A1406,A1412

A MODEL FOR THE TRANSPORT AND CHEMICAL REACTION OF MOLTEN DEBRIS IN DIRECT CONTAINMENT HEATING EXPERIMENTS*

K. D. Marx
Thermofluids Division
Sandia National Laboratories
Livermore, CA 94550

ABSTRACT

A computer model is described which simulates the effects of releasing molten debris into a gas-filled container. This work is motivated by studies of direct containment heating due to the dispersal of debris produced in certain nuclear reactor accident scenarios. The model consists of a finite-difference scheme for the gas flow coupled with a Lagrangian particle transport algorithm. It computes the transport of the debris through the gas and evaluates radiative and convective heat transfer effects. It also accounts for the chemical reaction of the debris with the oxygen in the atmosphere, including the concurrent heat release. The resulting computer code is used to simulate experiments in the Surtsey Direct Heating Test Facility. It is found that the computational results agree well with experiment for modest debris fluxes. It is further shown that the simulation of configurations with large fluxes can be improved with better submodels to describe the debris behavior. The description of the interaction of the debris with the container walls is of particular importance.

* This work was performed at the Combustion Research Facility and supported by the U. S. Nuclear Regulatory Commission.

Table of Contents

List of Illustrations

List of Tables

List of Symbols

Roman:

A_n	Projected area of particle
C_D	Drag coefficient
c_p, c_{pk}	Specific heat at constant pressure
c_v	Specific heat at constant volume
$C_{1\epsilon}, C_{2\epsilon}$	Coefficients in ϵ-equation
C_μ	Coefficient in eddy-viscosity formula
d, d_n	Particle diameter
D	Gas diffusion coefficient
D_{Dr}	Drop diameter
D_p	Particle diffusion coefficient
f_b	Bounce factor for particles
$\mathbf{F}_p$	Drag force on gas
$g, \mathbf{g}$	Gravitational acceleration
h_i	Specific Enthalpy of k^{th} species
I	Specific internal energy of gas
k	Turbulent kinetic energy
k_T	Thermal conductivity of the gas
M_{kn}, M_n	Mass of material in particles
Nu	Nusselt number
N_n^p	Particle weighting of n^{th} parcel
p	Pressure
Pr	Molecular Prandtl number
Pr_T	Turbulent Prandtl number
p_{drip}	Probability of particle dripping
p_{trap}	Probability of particle trapping
$\dot{q}_c$	Convective heat flow from particles
$\dot{q}_r$	Radiative heat flow from particles
q_w	Wall heat flux
$\dot{Q}_p$	Particle energy transfer to gas
$\dot{Q}_r$	Radiative heat transfer from gas to walls
r	Radial coordinate
R	Gas constant
Ra_x	Rayleigh number based on distance x
Re_p	Particle Reynolds number
Sc_T	Turbulent Schmidt number
Sh	Sherwood number
S_p	Particle surface area

List of symbols (cont.)

t	Time
t_{DS}	Dripping delay time
T	Gas temperature
T_p	Debris temperature
T_w	Wall temperature
$\mathbf{u}$	Mean gas velocity
$\mathbf{u}'$	(Normally distributed) turbulence intensity
u_*	Wall friction velocity
$\mathbf{v}_n$	Particle velocity
w_k	Molecular weight of k^{th} species
$\overline{w}$	Average molecular weight of gas
y	Perpendicular distance from wall
Y_i	Mass fraction
z	axial coordinate

Greek:

δ	Unit tensor
ΔV_{cell}	Volume of finite-difference cell
ε	Turbulence dissipation rate
ϵ_g	Gas emittance
ϵ_p	Particle emissivity
κ	Von Kármán constant
λ	Molecular thermal conductivity of gas
μ	Total viscosity
μ_L	Laminar viscosity
μ_T	Eddy viscosity
ρ	Total density
ρ_i	Density of i^{th} species
$\dot{\rho}_{pi}$	Species mass transfer source term
σ	Stress tensor
σ_ϵ	Schmidt number in ϵ-equation
σ_{SB}	Stefan-Boltzmann constant
τ_d	Time constant for drop-side reaction rate limit
τ_g	Time constant for gas-side reaction rate limit
τ_d	Overall time constant for reaction rates
τ_{TD}	Time constant for drop temperature decay

List of symbols (cont.)

Subscripts:

bl	Boundary layer
d	Debris
f	Final (steady-state)
fc	Free convection
g	Gas
i	Gas species
k	Particle species
lw	Law of the wall
n	Parcel index
o	Initial conditions
ox	Oxidation
p	Particle
T	Turbulence
w	wall

Superscripts:

g	Gas
T	Transpose of tensor

Abbreviations:

DCH	Direct Containment Heating

Acknowledgments

Many thanks are due K. D. Bergeron, D. E. Carroll, M. Pilch, W. W. Tarbell, K. E. Washington, and D. C. Williams for valuable discussions of various aspects of this project.

This work was supported by the Office of Nuclear Regulatory Research, United States Nuclear Regulatory Commission.

Executive Summary

This report describes work performed at Sandia National Laboratories, Livermore under the Sandia Direct Containment Heating Program for the U. S. Nuclear Regulatory Commission. A computer model has been developed which provides a numerical simulation of debris dispersal and heat transfer processes which occur in direct containment heating scenarios. Computational results are given for simulations of some experiments performed in the Surtsey Direct Heating Test Facility at Sandia Laboratories, Albuquerque.

The computer code was developed by making extensive modifications to the Kiva code, which was originally developed at Los Alamos National Laboratory to study spray combustion in engines. The spray model in the code has been adapted to the treatment of debris particle transport in the present applications. The resulting computer program will be referred to as Kiva-DCH.

The use of Kiva-DCH to study direct containment heating problems is intended to complement calculations carried out with the CONTAIN code. Kiva-DCH is capable of detailed modeling of relatively small and simple systems (e.g., experiments), whereas CONTAIN is a lumped-parameter code intended for the simulation of large systems (e.g., reactors). It is expected that the more accurate results from Kiva-DCH calculations will be used to refine the models used in CONTAIN. The simulation of very large systems is beyond the capabilities of Kiva-DCH due to computer limitations.

The results given in this report pertain to the DCH-1 (small total debris mass) and DCH-2 and DCH-3 (large total debris mass) experiments performed in the Surtsey facility. It is seen that the present version of the Kiva-DCH code has the capability of providing a good reproduction of the experimental pressure histories in these tests if enough detail is included in the physical models. The modeling of the interaction between the debris and the walls of the experimental vessel is seen to be of particular importance. It is treated in only an ad hoc way at present.

Future work to be addressed, in addition to debris-wall interactions, include the implementation of more chemical reactions and the modeling of more complex geometries.

I. INTRODUCTION

The transport and chemical reaction of debris is a problem of current interest in the study of certain nuclear reactor accident scenarios.[1] In some situations, debris from the core of a reactor could be expelled into the atmosphere inside a reactor containment building. The debris would then heat the gas, resulting in an increase in the pressure in the containment. Furthermore, the exothermic reaction of the debris with the oxygen in the air would cause additional heating of the atmosphere. The present work is part of a study being carried out to determine whether this heating will be sufficient to place the integrity of the containment building at risk due to overpressurization. We have developed methods for computer simulation of some of the physical processes involved in such direct containment heating (DCH) configurations. In this report, these numerical algorithms are used to model experiments pertinent to the reactor debris dispersal problem.

We consider multiphase flows in which small liquid and solid particles are dispersed in a gas-filled container. The particles may contain more than one chemical species. They are typically molten when injected into the gas, and then solidify either while propagating through the gas, or upon sticking to the surface of the container. In addition to heat transfer and phase change during transport, some of the constituents of the particles undergo chemical reaction with oxygen in the gas. The heat release due to this combustion process plays an important role in determining the gas pressure in the container.

The particle transport and heat transfer phenomena of concern in this work are closely related to similar processes considered in the study of the combustion of liquid fuel sprays.[2–5] For this reason, we have found it convenient to use a modified version of the Kiva computer code[2] to perform our calculations. Kiva has been developed at Los Alamos National Laboratory to simulate spray transport and combustion processes in internal combustion engines, and its spray model lends itself naturally to adaptation to the present debris model. Hence, this work provides a good example of application of technology from one area of combustion research to another. The numerical methods employed here are applicable to a variety of additional combustion modeling problems. These include the transport of aerosols and combustion-generated particulates, and the effects of convection and buoyancy in the propagation of fires.

A number of modifications have been made to Kiva to permit its use in the debris simulation problem. These include the following: (1) The characteristics of the liquid droplets were changed from a single species of evaporating liquid fuel to a multispecies distribution of nonevaporating metal particles. The injected liquid particles are allowed to solidify by implicitly including the heats of fusion in the enthalpy tables. (2) The algorithm for injecting the fuel droplets into the gas was modified to accommodate the specification of the initial species concentrations within the debris particles and the distributions of particle sizes and injection velocities. (3) Provision was made for the inflow of a compressed gas to drive the debris into the container. (4) A method for allowing the bouncing and trapping of particles at walls was introduced. (5) Algorithms were provided to account for radiative heat transfer, and for that component of convective heat transfer which occurs at length scales too small to be resolved on the finite-difference grid. (6) Allowance was made for chemical reactions between some of the chemical species in the particles and the oxygen in the atmosphere. (7) A model was included which permits the retention of debris mass on the upper surface of a container and its later dripping from that surface.

The resulting modified version of Kiva will be referred to as Kiva-DCH. It has been applied to the simulation of experiments performed in the Surtsey[6] facility at Sandia National Laboratories in Albuquerque, New Mexico. (See Figure 1.) The calculations have thus far been used only for the analysis of these experiments. However, it is expected that Kiva-DCH can also influence the development of models used in CONTAIN,[7] which is a lumped-parameter code being implemented in studies of full-scale reactor containment buildings. Kiva-DCH and CONTAIN will complement each other; Kiva-DCH can provide detailed studies of small, simple geometries which will help to define the capabilities and limitations of CONTAIN. Then CONTAIN can apply these results to improve the models that it uses in lumped-parameter simulations of full-scale containments, which could not be performed with Kiva-DCH because of the excessive computational resources required.

Some of the characteristics of the Kiva-DCH code are briefly described in Section II below. The most important of the modifications and additional physical models which have been included in the code to make it suitable for the debris simulation problem are described in Section III. Section IV provides a brief discussion of the Surtsey facility. In section V, we exhibit results of the computer calculations, and compare them with data from Surtsey experiments. Conclusions and proposed future work are presented in the final section.

II. COMPUTER CODE AND TURBULENCE MODEL

The basic Kiva code is described elsewhere.[2] In the interest of brevity, the equations which are solved by the code to describe the gas phase and its coupling to the debris are relegated to Table I and will not be discussed in detail here. The identification of the variables involved appears in the List of Symbols on Page xi. Some of the features of the equations and the numerical solution are outlined below. For further physical and computational details see Reference 2.

The Kiva code uses finite-difference approximations to solve Eqs. (1)–(5) (see Table I) for two- or three-dimensional flows; the present calculations are performed in two-dimensional axisymmetric cylindrical coordinates.

The gas temperature T is computed from the specific energy I by assuming that the species enthalpies h_i are functions only of T. Diffusion of mass and heat in the gas are accounted for by the terms involving the mean diffusion coefficent D and the thermal conductivity k_T. We are neglecting differential species diffusion by using an average value of diffusion coefficient D.

The eddy viscosity is obtained from the k-ϵ turbulence model as described in Jones[8] and Rodi.[9] Although Jones specifically addresses the question of compressible flows, it should be noted that turbulence models for compressible flows are not well-developed. Hence, the choice of the standard k-ϵ model in this situation cannot be regarded as definitive. The laminar viscosity is obtained from Sutherland's formula with appropriate coefficients, but is actually negligible in our calculations. The coefficients C_μ, $C_{1\epsilon}$, and $C_{2\epsilon}$ and the Schmidt number σ_ϵ are modeling constants. These constants have been tuned[9] for agreement with certain experiments, with

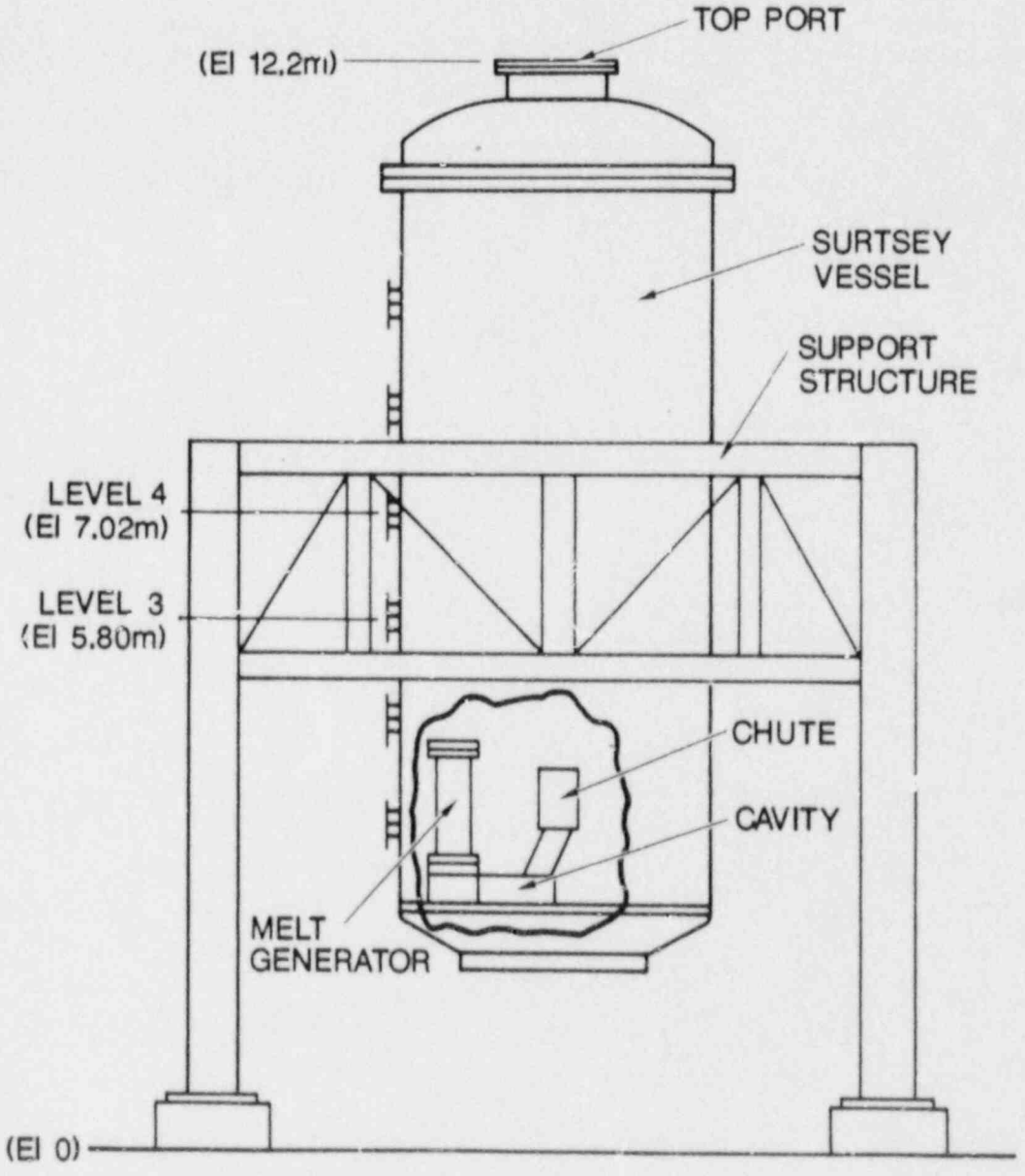

Figure 1. Schematic of the Surtsey Direct Heating Test Facility (taken from Reference 6). The DCH-1 apparatus is shown; the chute was removed for the DCH-2 experiment, but was in place for DCH-3.

TABLE I.

Reynolds-averaged equations for gas flow used in this work.

Mass conservation:

$$\frac{\partial \rho_i}{\partial t} + \nabla \cdot (\rho_i \mathbf{u}) = \nabla \cdot \left[D \nabla (\rho_i / \rho) \right] + \dot{\rho}_{pi} \tag{1}$$

$$\rho = \sum_i \rho_i \tag{1a}$$

Momentum conservation:

$$\frac{\partial (\rho \mathbf{u})}{\partial t} + \nabla \cdot (\rho \mathbf{u}\mathbf{u}) = -\nabla p + \nabla \cdot \sigma + \mathbf{F}_p \tag{2}$$

Energy conservation:

$$\frac{\partial (\rho I)}{\partial t} + \nabla \cdot (\rho I \mathbf{u}) = -p \nabla \cdot \mathbf{u} + \nabla \cdot \left[k_T \nabla T + \rho D \sum_i h_i \nabla (\rho_i / \rho) \right] + \dot{Q}_p + \dot{Q}_r + \rho \epsilon \tag{3}$$

Transport, production, and dissipation of turbulent kinetic energy:

$$\frac{\partial}{\partial t}(\rho k) + \nabla \cdot (\rho k \mathbf{u}) = \sigma : \nabla \mathbf{u} + \nabla \cdot (\mu \nabla k) - \rho \epsilon \tag{4}$$

Transport, production, and dissipation of turbulence dissipation rate:

$$\frac{\partial}{\partial t}(\rho \epsilon) + \nabla \cdot (\rho \epsilon \mathbf{u}) = C_{1\epsilon} (\sigma : \nabla \mathbf{u}) \frac{\epsilon}{k} + \nabla \cdot \left(\frac{\mu}{\sigma_\epsilon} \nabla \epsilon \right) - \frac{C_{2\epsilon} \rho \epsilon^2}{k} \tag{5}$$

Ideal gas law:

$$p = \frac{\rho R T}{\overline{w}} \tag{6}$$

TABLE I

(cont.):

Associated formulas:

$$Y_k = \rho_k / \rho \tag{7}$$

$$\sigma = -\frac{2}{3}\rho k \delta + \mu\left[\nabla \mathbf{u} + \nabla \mathbf{u}^T - \frac{2}{3}(\nabla \cdot \mathbf{u})\delta\right] \tag{8}$$

$$\mu = \mu_L + \mu_T \tag{9}$$

$$\mu_T = C_\mu \rho \frac{k^2}{\epsilon} \tag{10}$$

$$k_T = \frac{c_p \mu}{Pr_T} \tag{11}$$

$$D = \frac{\mu}{\rho Sc_T} \tag{12}$$

Boundary conditions on turbulence parameters at walls:

Zero normal flux condition on k:

$$\mu \nabla k \cdot \mathbf{n} = 0 \tag{13}$$

Law-of-the-wall condition on ϵ:

$$\epsilon = \frac{u_*^3}{\kappa y} \tag{14}$$

$$u_* = C_\mu^{1/4} k^{1/2}$$

optimum values $C_\mu = 0.09$, $C_{1\epsilon} = 1.92$, $C_{2\epsilon} = 1.44$, and $\sigma_\epsilon = 1.3$. Turbulent Prandtl and Schmidt numbers Pr_T and Sc_T are introduced (see Eqs. (11) and (12)) to model the turbulent heat and mass transfer in the gas. We have used $Pr = Sc = 0.70$.

All the computations employ an Eulerian method on a grid with rectangular cells. The z-axis coincides with the axis of the experimental facility to be modeled. In the computations presented in this report, the grid consists of 10 points in the (radial) r-direction by 20 points in the (axial) z-direction. This is a very coarse grid; it suffices only to resolve the largest eddies in the flow. We have investigated the numerical accuracy by refining the grid spacing for a typical problem by 50%. The resulting change in peak pressure was only 3%. Hence, the coarse grid suffices for the present calculations, in which the system is dominated by debris transport and heat transfer, and the large-scale gas flow plays a secondary role.

In the Kiva code, the boundary conditions on tangential gas velocity are obtained by implementing the law of the wall for turbulent boundary layers.[2,10,11] To this end, the tangential velocities at the walls are not set equal to zero, but are allowed to vary to account for fluid momentum in the wall grid cells, which are in the boundary layer. The boundary conditions on k and ϵ are are given in Table I.

III. PHYSICAL MODELS UNIQUE TO THE PRESENT CALCULATIONS

The previous section dealt primarily with the numerical model for the gas flow. Various terms appear in the fluid equations to account for the coupling to the liquid or solid phase, i.e., the debris particles. In this section, we discuss a number of physical models which were implemented for the purpose of the DCH simulations. Most of these have to do with the debris particles, although the definitions of the coupling term $\dot{\rho}_{pO_2}$ will be given and the method for treating gas-to-wall heat transfer will be discussed.

Debris Particles

The behavior of the debris is modeled by defining computational debris particles, referred to as "parcels."[2] A parcel behaves exactly as an individual debris particle would; however, the number of actual debris particles represented by the n^{th} parcel is a number N_n^p, which is usually larger than unity. When computing the influence of the particles on the gas, the effect of the n^{th} particle is multiplied by N_n^p. In this way, the debris can be represented statistically by a computationally feasible number of parcels. We let each parcel represent the same total debris mass as every other parcel. The associated particle diameter d_n varies from parcel to parcel. Hence, N_n^p is, in general, different for each parcel. In this work it varies from around unity to nearly 10^6.

The mass of the k^{th} species in the particle represented by the n^{th} parcel is denoted M_{kn}. The mass M_n of the particle is obtained by summing M_{kn} over all k. In the present work, we consider the 3 species Fe,FeO, and Al_2O_3. The equation of motion of the particles is given by

$$M_n \frac{d\mathbf{v}_n}{dt} = \frac{C_D \rho A_n}{2} \mid \mathbf{u} + \mathbf{u}' - \mathbf{v}_n \mid (\mathbf{u} + \mathbf{u}' - \mathbf{v}_n) + M_n \mathbf{g} \qquad (15)$$

The first term on the right is the drag force and the second is the gravitational force. For the purpose of computing the drag coefficient C_D (and the heat and mass transfer rates discussed below), the particles are assumed to be spherical.

The drag force term in Equation (2) is then written as

$$\mathbf{F}_p = -\frac{1}{\Delta V_{cell}} \sum_n^{cell} \frac{C_D \rho A_n}{2} \mid \mathbf{u} + \mathbf{u}' - \mathbf{v}_n \mid (\mathbf{u} + \mathbf{u}' - \mathbf{v}_n) N_n^p$$

where $\sum_n^{cell}$ means that the summation is to be carried out only over particles in the finite-difference cell where $\mathbf{F}_p$ is to be evaluated, and ΔV_{cell} is the volume of the cell.

Chemistry

Thus far, the particle treatment is similar to that appearing in the original Kiva code, except that in this case we are dealing with multispecies particles, rather than single-species fuel spray droplets. We now turn to the chemical reactions and heat transfer; these effects provide additional coupling between the debris and the gas, and require some new approaches.

The chemical reaction considered here is

$$2Fe + O_2 \longrightarrow 2FeO$$

Reaction of the iron in the debris with the oxygen in the atmosphere can be broken into two steps wherein (1) the oxygen molecules diffuse to the surface of the particle, and (2) the oxygen diffuses through the particle and oxidizes the metal. Hence, one can identify two diffusion limits to the reaction rate, referred to as the gas-side limit and the drop-side limit. It is assumed that these limits dominate any imposed by kinetics. Our method of evaluating the reaction rate subject to the diffusion limits is based on that discussed in Reference 1. The rate at which oxygen diffuses to the surface is assumed to be given by the following standard mass transfer formula.[1,12] (Henceforth, the parcel index n will be dropped for simplicity whenever possible.)

$$\dot{M}_{O_2} = \pi d D_{O_2} Sh \rho_{O_2} \tag{16}$$

where $\dot{M}_{O_2}$ is the mass of O_2 per unit time arriving at a single particle surface, d is particle diameter, D_{O_2} is the coefficient of diffusion of oxygen in air, ρ_{O_2} is the density of oxygen in the ambient atmosphere surrounding the particle, and the Sherwood number is given by [12]

$$Sh = 2.0 + 0.6 Re_p^{1/2} Sc^{1/3} \tag{17}$$

The quantities Re_p and Sc are the relevant molecular Reynolds and Schmidt numbers for the particle and the ambient air.

Given this rate of oxygen diffusion to the particle, a time constant τ_g can be defined describing the gas-side limit to the reaction rate:[1]

$$\tau_g = \frac{1}{2}\frac{w_{O_2}}{w_{Fe}}\frac{M_{Fe}}{\dot{M}_{O_2}} \tag{18}$$

The drop-side limit to the reaction rate is approximated by studying solutions to the diffusion equation for a spherical particle.[1] It has been determined that reasonably good results can be obtained by assigning a time constant

$$\tau_d = \frac{C_{d_s} d^2}{D_p} \tag{19}$$

where $C_{d_s} = 0.01107$ is an empirical constant, and D_p is the diffusivity of the particle. In all our work to date, we have used[1]

$$D_p = \begin{cases} 10^{-8} \ \text{m}^2/\text{s} & T_p \geq 1200\text{K} \\ 0 & T_p < 1200\text{K} \end{cases}$$

(Hence, the reaction is cut off when the particle temperature falls below 1200K.)

The gas-side and drop-side diffusion rates are implemented in the chemical reaction rate for a particle by writing

$$\frac{dM_{Fe}}{dt} = -\frac{M_{Fe}}{\tau_e} \tag{20}$$

where the effective reaction time constant τ_e is obtained from the following combination of the gas-side and drop-side diffusion times:

$$\tau_e = \sqrt{\tau_g^2 + \tau_d^2} \tag{21}$$

Strict mass conservation under chemical reactions is achieved by setting the rate for formation of FeO equal to

$$\frac{dM_{FeO}}{dt} = -\frac{w_{FeO}}{w_{Fe}}\frac{dM_{Fe}}{dt} \tag{22}$$

and by defining the mass source term for oxygen in (1) as

$$\dot{\rho}_{pO_2} = \frac{1}{2\Delta V_{cell}} \frac{w_{O_2}}{w_{Fe}} \sum_{n}^{cell} \frac{dM_{Fen}}{dt} N_n^p \tag{23}$$

(The factor 2 is the appropriate stoichiometric coefficient.)

Heat Release and Particle Heat Transfer

Conservation of energy during chemical reactions and heat transfer between particles and gas is accounted for by the equation

$$h_{Fe}(T_p)\frac{dM_{Fe}}{dt} + h_{FeO}(T_p)\frac{dM_{FeO}}{dt} + h^g_{O_2}(T)\frac{dM'_{O_2}}{dt} + \sum_k M_k c_{pk}\frac{dT_p}{dt} = \dot{q}_c + \dot{q}_r \tag{24}$$

The h'_ks are the specific enthalpies of the indicated species with the heats of formation present to account for the chemical heat release. These enthalpies are assumed to be functions of the particle or gas temperature, as appropriate. The term dM'_{O_2}/dt describes the rate at which oxygen is transferred to a single particle. The summation over species k in the rate of change of sensible heat refers only to the particle species; i.e., the mass and specific heat of the oxygen which is diffusing into the particle are neglected. Finally, $\dot{q}_c$ and $\dot{q}_r$ refer to convective and radiative heat transfer from the particle, which we now address.

The convective heat transfer is given by[12]

$$\dot{q}_c = -\frac{Nu\lambda S_p}{d}(T_p - T) \tag{25}$$

where λ is the thermal conductivity, $S_p = \pi d^2$ is the particle surface area, and the Nusselt number is (see the analogous Equation (17) for the Sherwood number)

$$Nu = 2.0 + 0.6Re_p^{1/2}Pr^{1/3}$$

with Pr denoting the molecular Prandtl number for the gas.

We use the following model for the radiative term:

$$\dot{q}_r = -\epsilon_p \sigma_{SB}(T_p^4 - T^4)S_p \tag{26}$$

where ϵ_p is the emissivity of the particles (assumed to be a single constant throughout the calculation), and σ_{SB} is the Stefan-Boltzmann constant. This formula requires that the optical thickness of the gas be great, so there is no appreciable radiation from the particles to each other or to the walls. In fact, the gas itself is not necessarily optically thick in these experiments; however, there is a significant amount of aerosol suspended in the gas which renders it opaque.

(The aerosol mass is only a few percent of the total debris mass, so it does not contribute significantly to the total debris heat capacity.) For the purposes of this paper we have assumed that the particles are black bodies, i.e., $\epsilon_p = 1$. The resulting particle radiation model is believed to be reasonable,[13] but it should be recognized that it is only an approximation.

Using (22) and a similar formula for dM'_{O_2}/dt, along with (25) and (26), Equation (24) provides an equation for the evolution of the particle temperature:

$$\sum_k M_k c_{pk} \frac{dT_p}{dt} = -h_{rr} \frac{dM_{Fe}}{dt} - \left(\frac{Nu\lambda}{d} + \epsilon_p \sigma_{SB} T_r^3 \right) \left(T_p - T \right) \tag{27}$$

where

$$h_{rr} = h_{Fe}(T_p) - \frac{w_{FeO}}{w_{Fe}} h_{FeO}(T_p) + \frac{1}{2} \frac{w_{O_2}}{w_{Fe}} h^g_{O_2}(T) \tag{28}$$

and

$$T_r^3 = \left(T_p^2 + T^2 \right) \left(T_p + T \right) \tag{29}$$

The term dM_{Fe}/dt in (27) is given by Equation (20). The energy source term $\dot{Q}_p$ in (3) is obtained by applying energy conservation to the preceding formulation.

Debris-Wall Interaction

We have used only an ad hoc treatment of the interaction of the debris particles with the walls. When a particle strikes the lower surface (floor) of the container, it always stays there and is taken out of the calculation. If it strikes any other surface, it is trapped on the surface with a probability p_{trap}. In the fraction $(1\text{-}p_{trap})$ of all encounters in which it is not trapped, it undergoes specular reflection, but with its reflected velocity reduced by a factor f_b.

Except for those particles which strike the upper wall (the dome of the facility), the fraction p_{trap} of particles which are trapped on walls are taken out of the calculation in the same way as those which strike the floor. However, it has been observed that debris material which strikes the dome has a tendency to remain there for a short period of time and then drip down. In anticipation of this, we have implemented the following special treatment for particles trapped on the dome in some calculations. When a debris particle is trapped on the dome, it is collected in a "dripping pool" with probability p_{drip}. In other words, the probability that a particle trapped on the dome is taken completely out of the calculation is $1 - p_{drip}$, but for a fraction p_{drip} of all such particles, the material in the particles will be part of a drop that falls later. (See Figure 2.) The diameter of these drops is an input parameter D_{Dr}. The drop material is collected until there is enough to form a drop of this size. Furthermore, in any case, the drop is retained on the dome until a time t_{DS} elapses from the time the first particle which goes into the formation of the drop strikes the dome. In practice, we have chosen t_{DS} = 2s, the debris injection time is

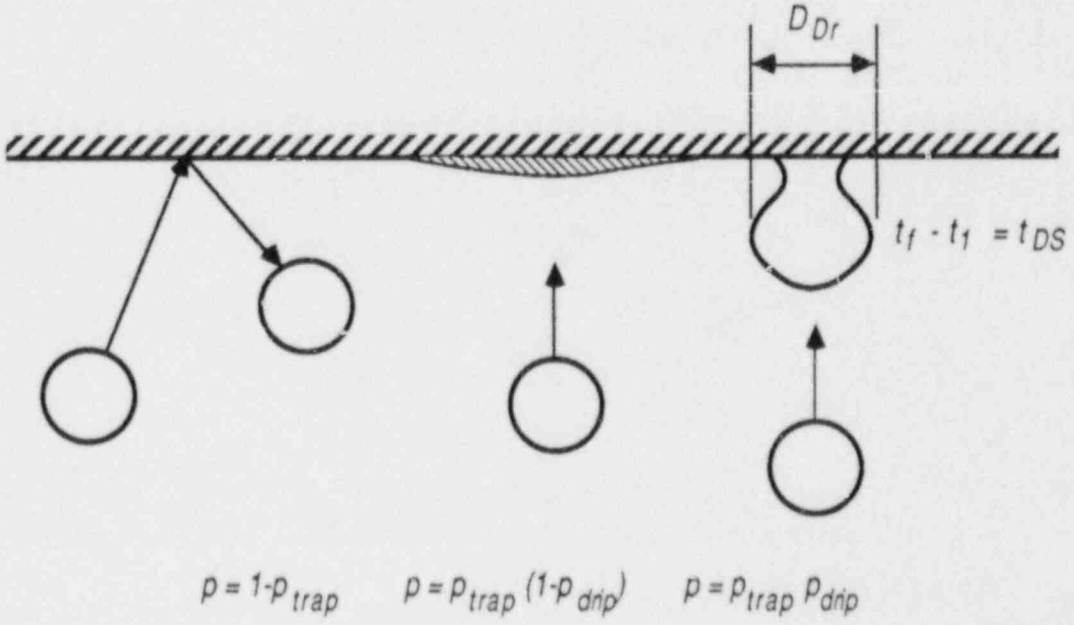

Figure 2. Schematic representation of the debris-wall interaction currently used in the calculations. Particles are always trapped when they strike the floor ($p_{trap} = 1$ there). Dripping is allowed only from the dome ($p_{drip} = 0$ elsewhere). The time t_f at which a drop falls is t_{DS} later than the arrival time t_1 of the first particle to go into the formation of the drop.

0.64s, and the particle transit time from chute to dome is of the order of 0.1s, so no drops fall before the collection into the trapping pool is complete.

Provision has been made for the debris to give up energy to the dome while stuck in the trapping pool. Material in the particles is allowed to cool with a time constant τ_{TD}. (However, the time constant has been set to infinity for all the results presented in this report.)

The quantities p_{trap}, f_b, p_{drip}, t_{DS}, D_{Dr}, and τ_{TD} used thus far have only been estimates. This is clearly a crude (and temporary) model. We will return to this subject below.

Heat Transfer from Gas to Walls

Finally, we describe the heat transfer from the gas to the walls. As pointed out in the discussion following Equation (26), it is assumed that there is sufficient aerosol suspended in the gas to cause it to appear optically thick. Hence, for the radiative contribution, we simply set the source term $\dot{Q}_r$ in (3) equal to

$$\dot{Q}_r = -\frac{\epsilon_g \sigma_{SB} A}{V}\left(T^4 - T_w^4\right) \tag{30}$$

where A is the total surface area of the container walls, V is the container volume, T_w is the wall temperature, and ϵ_g is the effective emittance of the aerosol-laden gas. (Strictly speaking, for (30) to hold, the absorptance of the gas to radiation from the walls should be equal to ϵ_g as well.[14]) We have used $\epsilon_g = 0.8$ for the present calculations.[15] In effect, use of Equation (30) amounts to applying a formula for a radiating gas in thermal equilibrium[14] by assuming that the equilibrium value of T^4 is equal to the average value of T^4 and then computing the volumetric source term $\dot{Q}_r$ with a T^4 weighting. This approximation yields good results when computed cooling rates are compared with those observed in experiments in the Surtsey facility. (See Section V.)

In principle, a fluid dynamics code should take care of convective heat transfer automatically by simulating the convective flux. In practice, in a configuration such as this, thermal boundary layers appear on the walls which are much too thin to resolve on a practical finite-difference grid. In the present problem, heat transfer through these boundary layers accounts for about half the heat loss from the gas. (The radiative contribution makes up the other half.) To accommodate this effect, we have implemented the following scheme, in which energy is taken out of finite-difference cells next to the walls in a way consistent with results from experiments on turbulent boundary layers.

For free convection, an appropriate correlation for the Nusselt number for a turbulent thermal boundary layer on a wall is [16]

$$Nu_x = C_t Ra_x^{1/3} \tag{31}$$

where C_t is an empirical constant, and Ra_x is the Rayleigh number based on x, the distance along the wall from the origin of the boundary layer. (Subscript x refers to that distance.) When

formulating the heat flux to the wall q_{fc} from this Nusselt number, the distance x cancels out, and one obtains

$$q_{fc} = \frac{C_t \lambda (T_1 - T_w)}{L_b} \tag{32}$$

where

$$L_b = \left[\frac{\nu^2 T_1}{Prg(T_1 - T_w} \right]^{1/3} \tag{33}$$

and ν and T_1 are the kinematic viscosity and the temperature of the gas outside the boundary layer.

The original Kiva code is set up to evaluate the wall flux by applying Reynolds' analogy to a law-of-the wall boundary layer (i.e., forced convection). We evaluate q_{fc} by taking T_1 as the temperature in the finite-difference zone next to the wall, and then set the wall flux equal to

$$q_w = \max(q_{fc}, q_{lw}) \tag{34}$$

where q_{lw} is the law-of-the wall formula. In the present case, q_{fc} nearly always dominates, except at early times when $T_1 \approx T_w$ and the velocities are high.

Blowdown Gas

To model the inflow of the nitrogen gas which is used to help drive the debris through the chute into the facility, appropriate boundary conditions are implemented at the mouth of the chute. The blowdown gas velocity there was obtained from information provided by Reference 17. Simulations of experiments with two different total input debris masses will be discussed below. The velocity history imposed for simulations of the experiment at lower total mass (DCH-1) is given in Figure 3. The velocity for the experiment at higher mass (DCH-2/DCH-3) is identical in form to that shown, but is increased by a factor of 1.8.

IV. THE EXPERIMENT

The Surtsey facility[6] is illustrated in Figure 1. It basically consists of a cylindrical vessel 10 m high by 3.7 m in diameter. In our finite-difference model it is assumed to be a right circular cylinder, i.e., the rounded surfaces at the ends are taken to be flat. In the experiments conducted in the facility thus far, the debris has been formed in a melt generator positioned as shown. The melt generator is filled with a thermite mixture consisting of magnetic oxide, Fe_3O_4, and powdered aluminum. When the thermite is ignited, it reacts to form a molten mixture of iron and alumina, Al_2O_3, and this debris is ejected out through a cavity into the atmosphere of

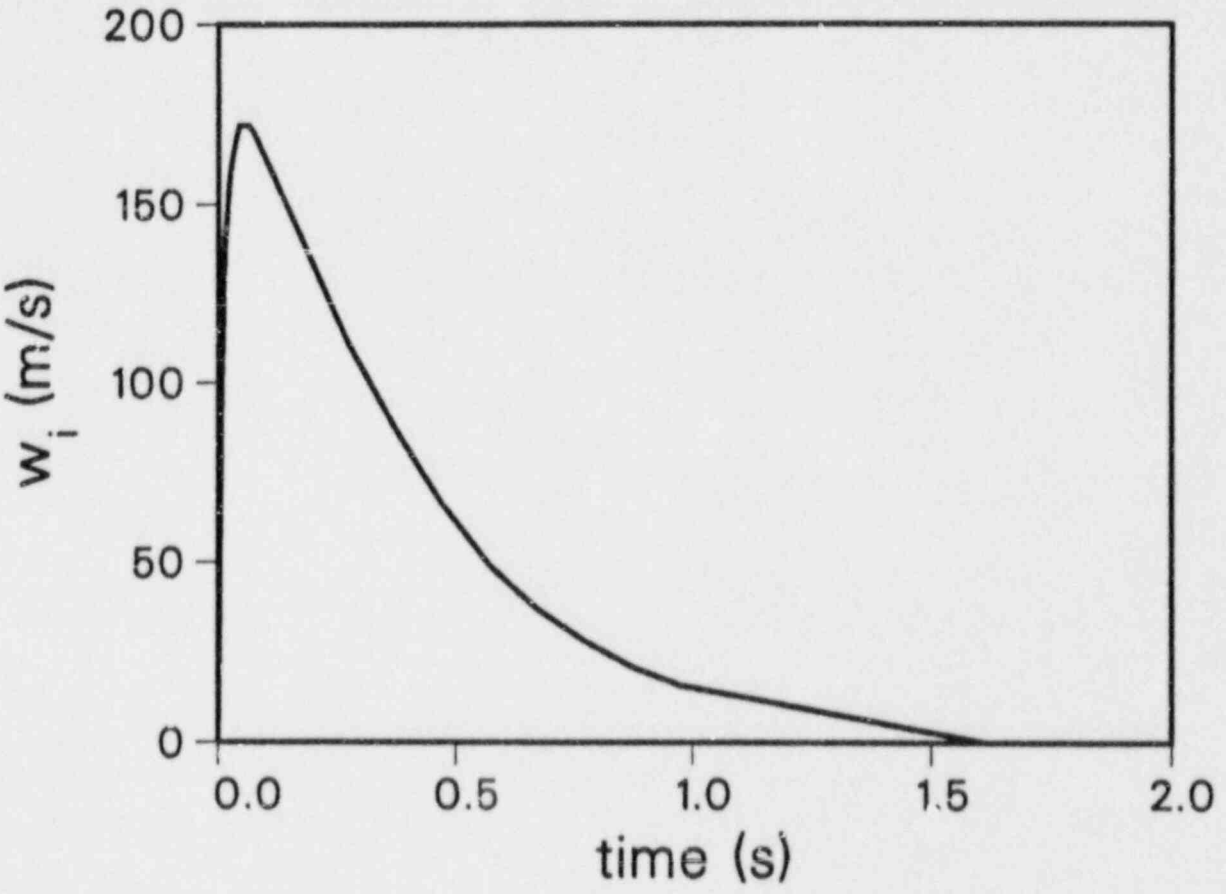

Figure 3. Blowdown gas velocity versus time used in simulations of the DCH-1 experiment. That used for DCH-2/DCH-3 consisted of the same function multiplied by a factor of 1.8.

the facility. The ejection is driven by compressed nitrogen gas which is released into the melt generator. (The inflow of the driving gas is simulated in our computations.)

Measurements have indicated that the mass of the injected debris is distributed among liquid droplets with a log-normal distribution in particle diameter[6] having median diameter 0.55 mm and standard deviation 4.2. This distribution is employed in the injection routine in the code, except that a lower and upper cutoff in particle diameter is assumed at $d = 0.04$ mm and $d = 4$ mm. The Sauter mean diameter of the particles is then 0.27 mm.

V. RESULTS

In this report, computational results will be compared with those from two experiments. In the first[6] (denoted DCH-1) the total mass of the injected debris was 9.5 kg. The flow of debris out of the cavity was directed upwards by means of the chute shown in Figure 1. In the second[18] (denoted DCH-2) the mass of the debris was 80 kg, and the chute was removed, so that the debris flow was directed toward the wall of the facility. This latter configuration is 3-dimensional. Our simulation is 2-dimensional, with the debris directed upward as if the chute were in place. Hence, it is actually a better simulation of Experiment DCH-3[19], and the results may be compared with DCH-3 data when the latter are available.

Results for the DCH-1 Experiment

The parameters which were used to model Experiment DCH-1 are given in Table II. Pressure histories from calculations with and without chemical reactions are shown in Figure 4; appropriate experimental data are given in Figure 4 for comparison. (Note: $p_{drip} = 0$; i.e., dripping from the dome was not allowed in this calculation.) Heat release from oxidation is seen to increase the peak pressure by about 40%. (This effect would be even more dramatic if the more exothermic reactions involving zirconium from a reactor core were involved.) The differences observed between computed and experimental rise times and peak pressures are modest, considering the complexity of the processes involved. The causes of these discrepancies are currently unknown. Corresponding particle plots and isotherms from the calculation with chemical reactions are provided in Figure 5. A key point to note in Figure 5 is that the temperature rise of the gas is not dramatic; high temperatures are confined to a small core on the axis. This reason for this is that the total heat capacity of the particles is relatively small in this case; a significant fraction of their heat is removed during one transit through the container. In particular, most of them freeze before striking a surface.

A Simple Model for DCH-1

We will now demonstrate that one can obtain a fairly good estimate of the above results for peak pressure in DCH-1 by performing a simple calculation based on thermal equilibration of the debris and gas. Let the total mass, specific heat, and initial temperature of gas be M_g, c_{vg}, and T_o, respectively. Similarily, the corresponding quantities for the debris will be denoted M_d, c_{vd}, and T_{do}. Let the heat released per unit mass of iron oxidized be Δh^{Fe}_{ox}. Further denote the initial

Table II.

Parameters Used in the Calculations

Initial gas temperature T_o	300K
Initial gas pressure p_o	0.083 MPa
Driving gas	N_2
Peak driving gas inflow velocity	172 m/s (DCH-1)
	310 m/s (DCH-2/DCH-3)
Driving gas inflow temperature	450K
Driving gas blowdown time	1.5 s
Initial debris composition (by weight)	47% Al_2O_3
	53% Fe
Initial debris temperature T_{po}	2500K
Total debris mass	9.5 kg (DCH-1)
	80 kg (DCH-2/DCH-3)
Mean debris inflow velocity	72 m/s
Debris injection time	0.64 s
Debris Sauter mean diameter D_s	0.27 mm
Standard deviation of random debris injection angle σ_θ	11.4° (exception noted below)
Trapping probability p_{trap}	0.05 (DCH-1)
	0.5 (DCH-2/DCH-3 w/o dripping)
	0.9 (DCH-2/DCH-3 w/ dripping)
Reflected velocity fraction f_b	0.8
Turbulence parameters Pr_T and Sc_T	0.70
Particle emissivity ϵ_p	1.0
Gas emittance ϵ_g	0.8

Calculation with dripping only:

Dripping probability p_{drip}	0.5
Dripping delay time t_{DS}	2s
Drop diameter D_D	0.25 cm
Drop cooling time τ_{T_D}	0.25 cm
Standard deviation of random debris injection angle σ_θ	5.7° (exception noted below)

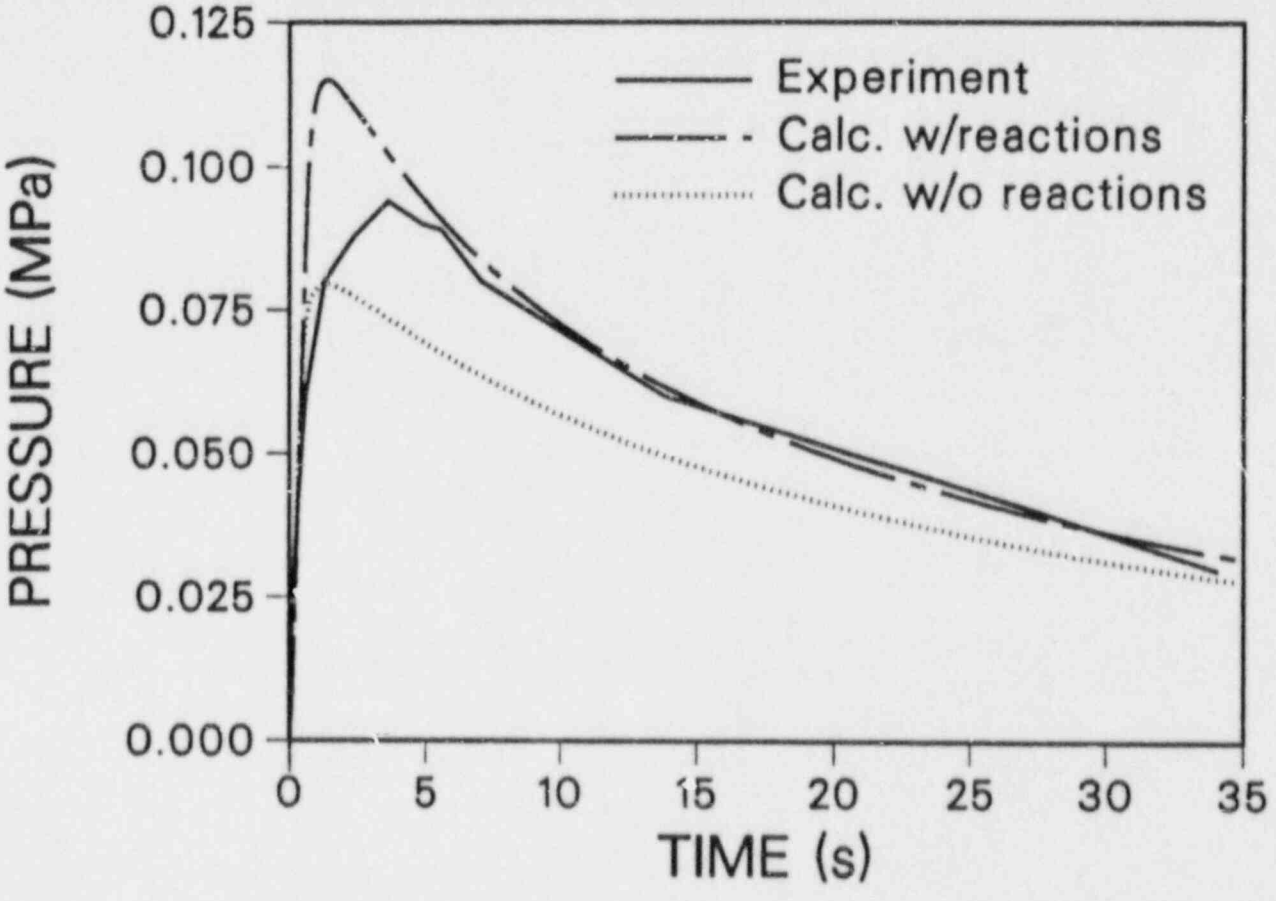

Figure 4. Results of simulations of the DCH-1 experiment. A computation made with the chemical reactions turned off is shown to illustrate their importance. Experimental data taken at Level 4 in the Surtsey facility (see Figure 1) is shown for comparison.

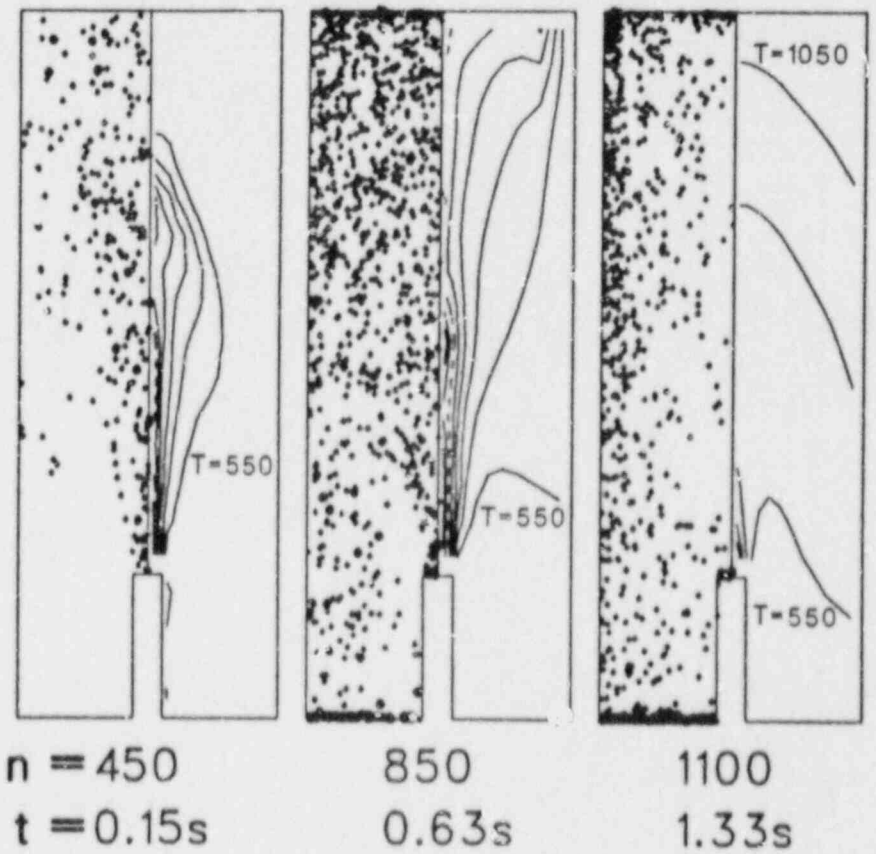

Figure 5. Particle plots (left) and isotherms (right) from 3 different times in the DCH-1 simulation. (The line dividing the two plots in each figure is the z-axis of the axisymmetric configuration.) The particle plots represent computational parcels (see text) existing within a thin pie-shaped wedge (the wedge angle is 0.5°). Only half of all the parcels are shown. Particles trapped on surfaces are displayed in the plot, but are removed from the calculation. The temperature levels of the isotherms are separated by 250K. The dashed isotherm represents 1800K, approximately the melting point of iron. The index n denotes the number of time steps elapsed.

mass fraction of iron in the debris by Y_{Fe} and assume that a fraction f_{oz}^{Fe} of this is oxidized. Now assume that the debris and the gas are mixed and come to thermal equilibrium without cooling. Assuming that all quantities are approximately invariant with temperature, energy conservation results in the following equation involving the final temperature T_f:

$$M_g c_{vg}(T_f - T_o) + M_g c_{vd}(T_f - T_{do}) = f_{oz}^{Fe} Y_{Fe} M_d \Delta h_{oz}^{Fe}$$

or

$$T_f = \frac{M_g c_{vg} T_o + M_d c_{vd} T_{do} + f_{oz}^{Fe} Y_{Fe} M_d \Delta h_{oz}^{Fe}}{M_g c_{vg} + M_d c_{vd}} \tag{35}$$

The ideal gas law (6) can then be used to evaluate the equilibrium pressure p_f.

For the DCH-1 experiment, we have M_g = 98 kg, M_d = 9.5 kg, Y_{Fe} = 0.53, and T_o = 300 K. Reasonable estimates for the other quantities (which are less easily determined) are $c_{vg} \cong$ 720 J/(kg · K), $c_{vd} \cong$ 1300 J/(kg · K), T_{do} = 2500 K, and $\Delta h_{oz}^{Fe} = 4.9 \times 10^6$ J/kg.

From (35) and (6) we obtain the following results which bracket the effects of chemical reaction:

$$f_{oz}^{Fe} = 0 \quad \longrightarrow \quad p_f = 0.090 \text{ MPa gauge}$$

$$f_{oz}^{Fe} = 1 \quad \longrightarrow \quad p_f = 0.172 \text{ MPa gauge}$$

From the numerical calculation with oxidation (solid line in Figure 4), it is found that the final oxidation fraction is f_{oz}^{Fe} = 0.37. An a posteriori calculation thus yields

$$f_{oz}^{Fe} = 0.37 \quad \longrightarrow \quad p_f = 0.121 \text{ MPa gauge}$$

This is close to the peak value of 0.115 MPa given by the solid line in Figure 4. Such close agreement is actually somewhat fortuitous. We arrived at Equation (35) by making a number of approximations. Among others, we ignored the fact that the injection of the driving gas would increase the final pressure. (A crude calculation places the magnitude of this effect at about 15% of the final absolute pressure.) The point is, however, that one can make a reasonably good estimate of the direct heating effect in this case.

Results for the DCH-2/DCH-3 Experiments

As noted above, the other experiments (DCH-2 and DCH-3) for which a simulation was performed is similar to DCH-1, except that 80 kg of debris was injected into the container, the amount of driving gas was increased (see Table II), and in the case of DCH-2 the debris was ejected toward the side wall. Results of a direct application of the same model used for DCH-1

to a simulation with debris mass of 80 kg are shown as the dashed curve in Figure 6. (Note in particular that p_{drip} is still set equal to zero in this case.) We see that the calculation predicts a very high peak pressure compared to experiment. But we know that it is not consistent to use a trapping probability of 0.05 in this case, because (contrary to DCH-1) the computation predicts that a significant amount of the debris mass is still molten when it strikes the surfaces of the container. (The reason for this is that the total heat capacity of the debris is much greater in DCH-2; see the discussion to follow.) There is evidence[19] that molten debris will predominantly stick to surfaces, at least for some period of time. Because of the low trapping probability, the amount of hot debris which remains in transit through the gas after striking the walls is overestimated, and the heat transfer to the gas is accordingly overpredicted. Note that this overestimation is a result of debris-wall interactions and heat transfer, and is not particularly sensitive to the difference in geometry (i.e., absence of the debris-directing chute).

To reflect the fact that in reality more debris will adhere to the walls than predicted above, another calculation was carried out for DCH-2/DCH-3 with p_{trap} increased to 0.5. The pressure history (see Figure 6) is now closer to the experimental result. Figure 7 shows the corresponding particle plots and isotherms. The region in which the gas temperature exceeds the melting point of iron is much more extensive than that shown in Figure 5. This is not surprising; we note it here to reinforce the point that the debris in this case will remain molten when it strikes the surfaces of the container. The much higher total heat capacity of the particles in this case has resulted in a thermal saturation effect. Not only will the temperatures remain higher because of the increase in the ratio of the heat capacity of the debris relative to that of the gas, but the *rate* at which the debris is cooled by the gas will be diminished, especially because of the nonlinearity (i.e., the T^4 term) in the radiative cooling law.

The Effect of Dripping from the Dome

As noted above, it is believed that appreciable amounts of debris stick to the dome of the facility and then drip down after a brief delay time. To illustrate the effect of such behavior, a DCH-2/DCH-3 simulation was carried out with $p_{trap} = 0.9$, $p_{drip} = 0.5$, $t_{DS} = 2s$, $D_{D_r} = 0.25$ cm, and $\tau_{TD} = \infty$. In this calculation, the debris ejection cone at the mouth of the chute was also narrowed. This was done by reducing the standard deviation of the randomly selected injection angle σ_θ from 11.4° to 5.7°

The resulting pressure history is given as the chain-dashed line in Figure 6. Particle plots and isotherms appear in Figures 8 and 9. The velocity field at $t = 0.585$ is shown in Figure 10. Note that the computed velocity field consists of a rather simple circulation pattern. The eddy viscosity computed from the $k - \epsilon$ model smooths out any tendency for the flow pattern to form the smaller eddies which exist in the experiment. In principle, the computational model accounts for them through the eddy viscosity. As noted in Section II, we have refined the finite-difference grid with no significant change in the pressure histories. The reason that the results do not depend sensitively on a careful resolution of small eddies is that in the Surtsey configuration, the pressure behavior is dominated by thermodynamics and large-scale heat transfer. The small-scale features of the flow have a lesser effect.

Since blowdown gas is being injected, the flow pattern is not that of an incompressible gas. (Note, however, that the mass flow rates are weighted by the radius r because of the

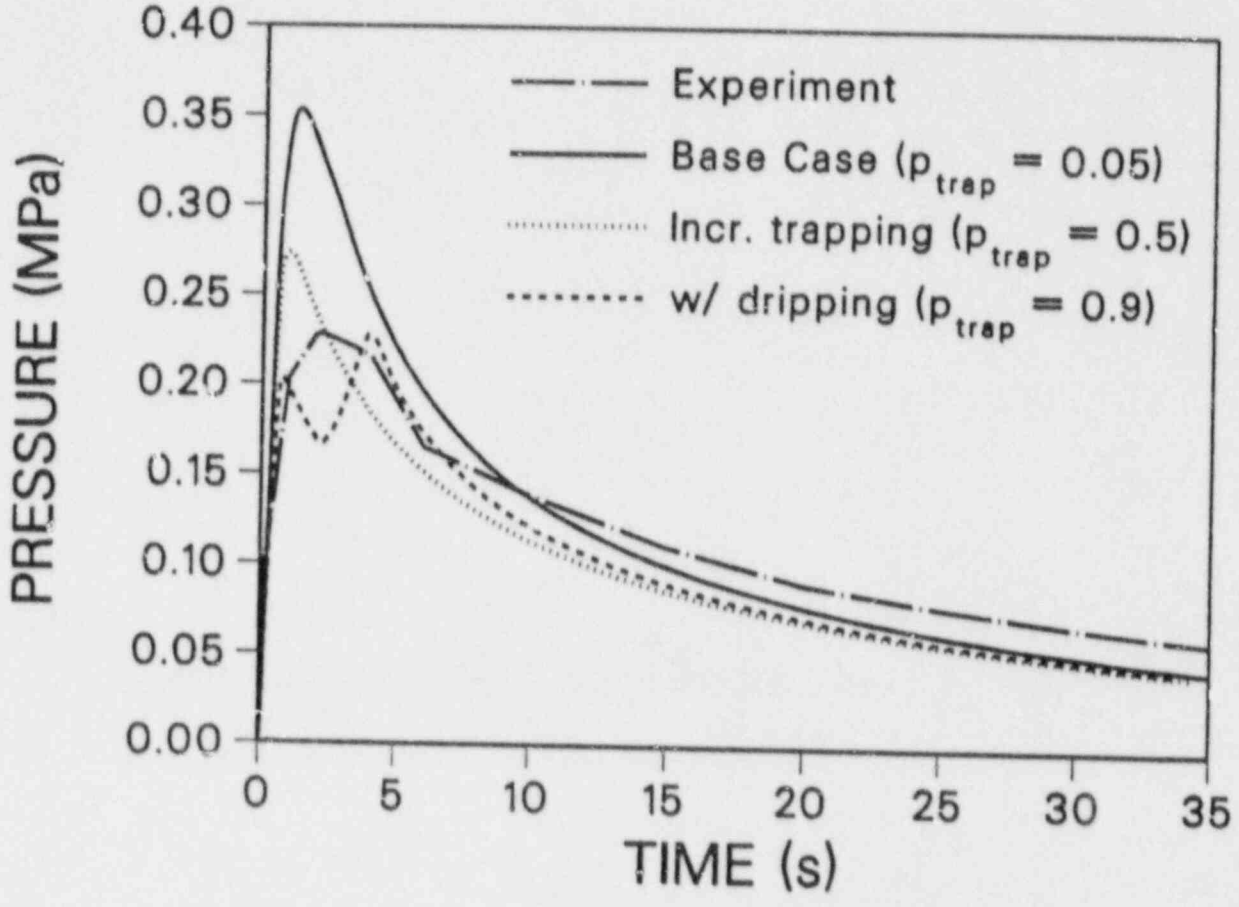

Figure 6. Results of simulations with mass flux and driving gas appropriate to the DCH-2 and DCH-3 experiments, with experimental data from DCH-2 at Level 3. Trapping probabilities equal to 0.5 or 0.9, rather than 0.05, are more realistic in this case because a greater amount of debris remains molten at the time it strikes the surface.

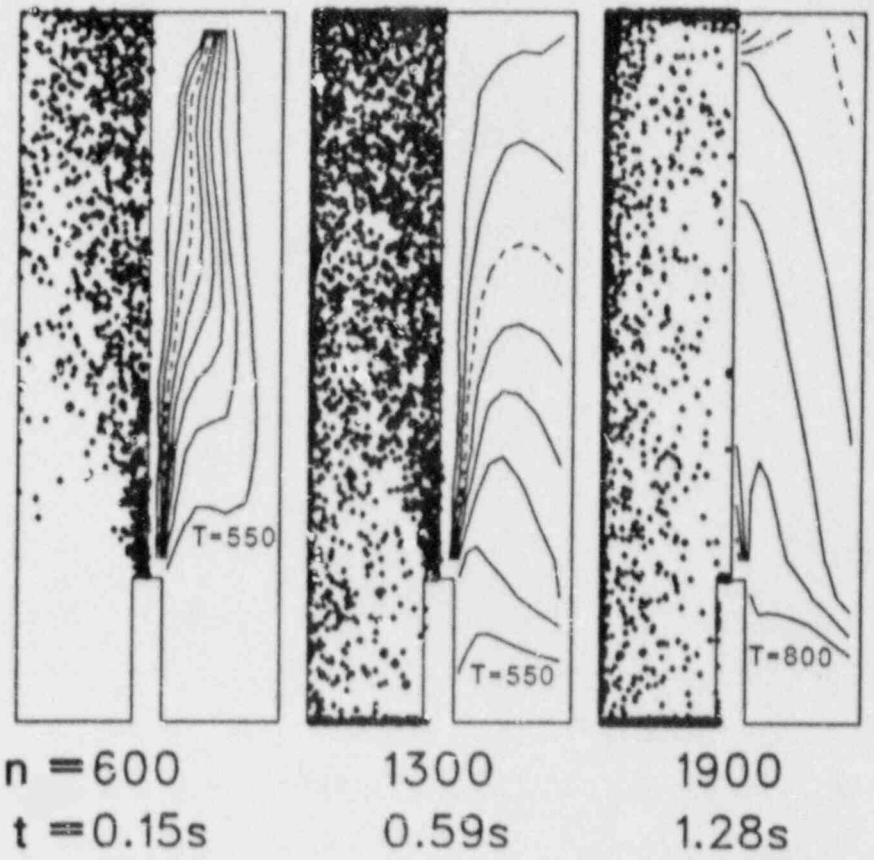

Figure 7. Particle plots and isotherms from the DCH-2/DCH-3 simulation with $p_{trap} = 0.5$. (See caption under Figure 5 for explanation.) Note that the hot core on the axis in the first two plots is more extensive than it is in DCH-1 (see Figure 5).

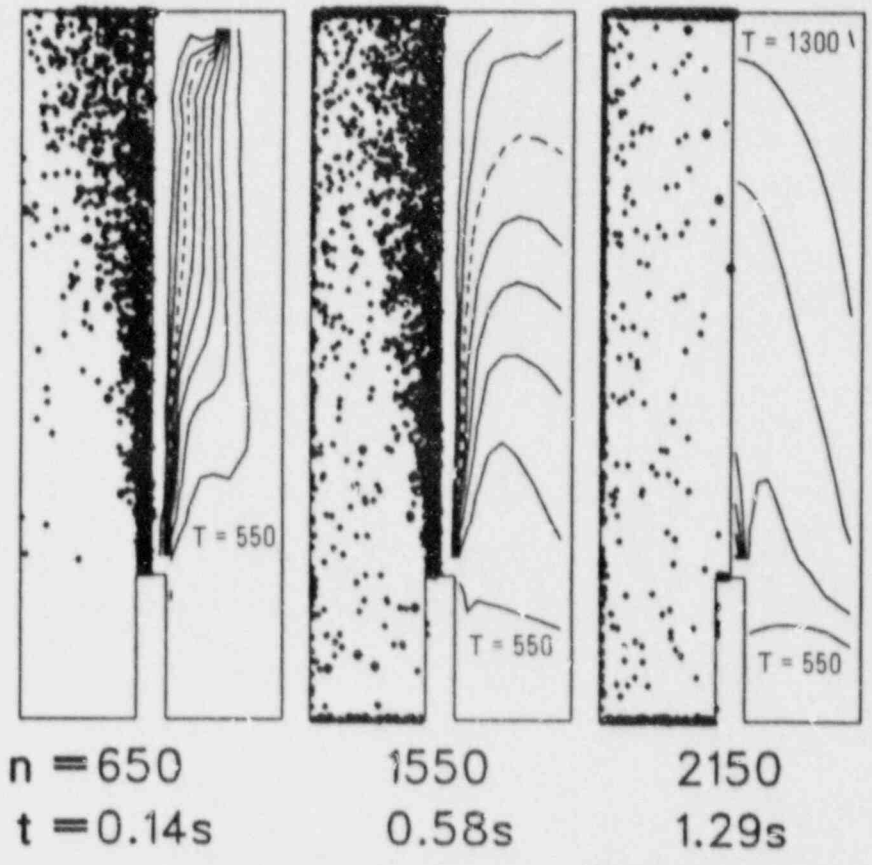

Figure 8. Particle plots and isotherms at early times from the DCH-2/DCH-3 simulation with dripping from the dome (For this computation, $p_{trap} = 0.9$, $p_{drip} = 0.5$, and $t_{DS} = 2$s. Also, the injection cone was made narrower in this case than in the calculation shown in Figure 7. See text.)

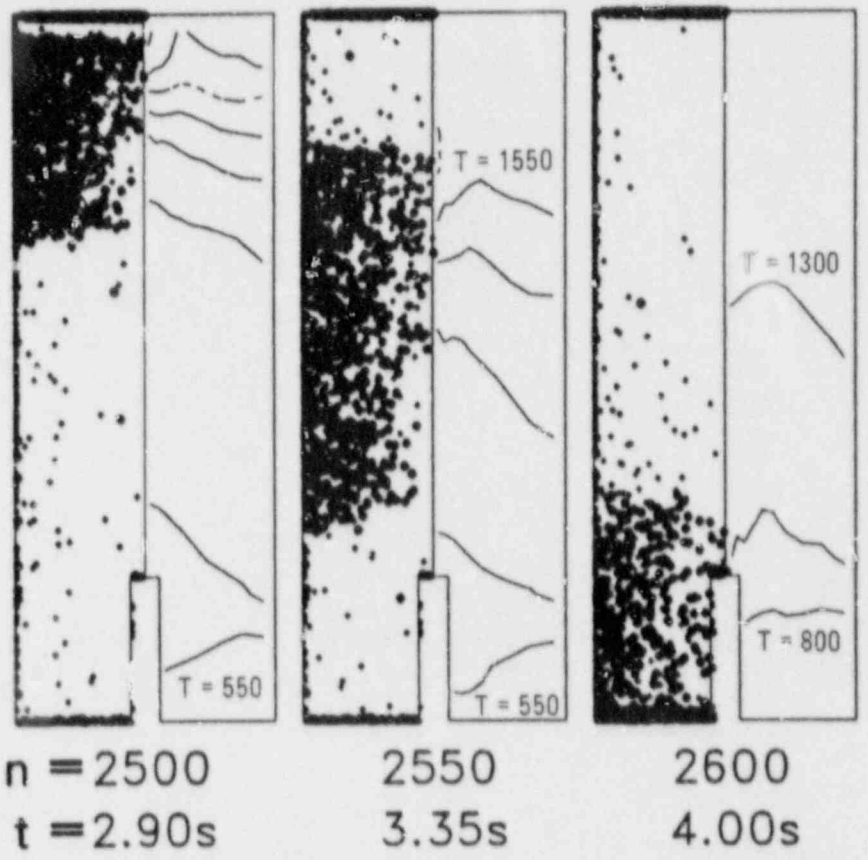

Figure 9. Particle plots and isotherms during dripping for the simulation shown in Figure 8.

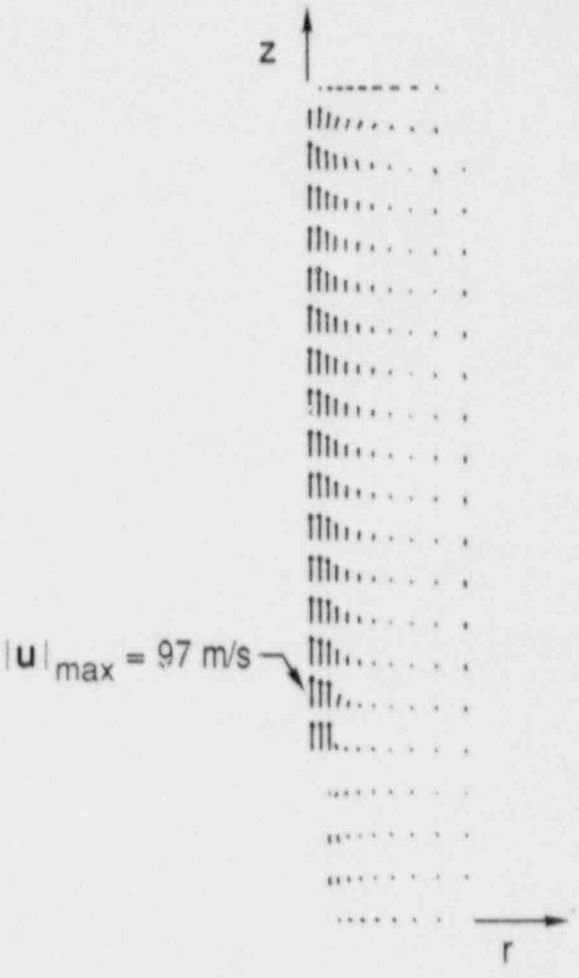

Figure 10. Velocity vectors at $t = 0.58$s (near the end of debris injection) for the simulation shown in Figure 8.

cylindrical geometry. Hence, the small velocity vectors near the outer wall account for a greater mass flow relative to the large velocity vectors on the axis than would appear at first sight.)

The Influence of Oxygen Depletion on Oxidation Rate

It is if interest to determine whether the depletion of oxygen in regions occupied by debris is important in determining the amount of debris oxidized in these experiments. We now present results which provide some insight into that question. Diagnostics have been implemented in Kiva-DCH which permit the display of the rate of oxidation under eight different assumptions. In the remainder of this subsection, these different rates are first defined, and then some representative computational results are given.

The code is run in the usual manner (except that we keep track of the blowdown gas separately from the ambient nitrogen, as discussed below). At the times at which data dumps are taken for input to the graphics postprocessor, the following rates of consumption of oxygen are computed (rates $\dot{\rho}^i_{O_2}$ have units of mass per unit volume per unit time):

1. The actual rate $\dot{\rho}^1_{O_2}$ computed and used in the simulation.

2. The rate $\dot{\rho}^2_{O_2}$ which would occur if the ratio of the density of O_2 to the density of ambient N_2 was equal to the initial ratio. In other words, the rate is computed under the assumption that the density of O_2 is given by

$$\rho^2_{O_2} \equiv \left(\frac{\rho^o_{O_2}}{\rho^o_{N_2}}\right)\rho_{N^a_2}$$

where superscript o refers to initial values and $\rho_{N^a_2}$ is the current computed density of the ambient nitrogen. By ambient nitrogen we mean the nitrogen that was originally in the container (excluding the blowdown gas). We keep track of the ambient and blowdown nitrogen by considering them as separate species in the code (but both with the properties of nitrogen).

This definition of $\rho^2_{O_2}$ is equivalent to saying that the mole fraction of O_2 (when the blowdown gas is excluded) is equal to the initial mole fraction. It provides a way to assess the effect of consumption of O_2 through oxidation on the rate of reaction. Comparison of $\dot{\rho}^2_{O_2}$ with $\dot{\rho}^1_{O_2}$ shows the difference between the rate which would exist if no oxidation had occurred and the actual rate which does exist. (This ignores, of course, the differences in the flow field which result from the removal of oxygen from the air.)

3. The rate $\dot{\rho}^3_{O_2}$ which would occur if the blowdown gas which exists at every point were replaced by a gas mixture with components in the same ratio as those which currently exist, excluding the blowdown gas. Hence, in this case it is assumed that the density of O_2 is

$$\rho^3_{O_2} \equiv \rho_{O_2} + X^3_{O_2} M_{O_2} n_{N^b_2}$$

where $n_{N^b_2}$ is the particle density of the blowdown gas and $X^3_{O_2}$ is the mole fraction of oxygen for the mixture excluding the blowdown gas:

$$X^3_{O_2} = \frac{n_{O_2}}{\sum_k{}' n_k}$$

The symbol $\sum_k{}'$ implies that the sum excludes the blowdown gas; the particle densities are

$$n_k = \frac{\rho_k}{M_k}$$

Comparison of $\dot{\rho}^3_{O_2}$ with $\dot{\rho}^1_{O_2}$ provides an indication of the effect on reaction rate due to the displacement of the ambient gas by the blowdown gas.

4. The rate $\dot{\rho}^4_{O_2}$ which would occur if the density of oxygen were equal to the initial density of oxygen. Hence, we use

$$\rho^4_{O_2} \equiv \rho^o_{O_2}$$

During the injection of the debris, not enough time elapses for thorough thermal mixing to take place. The gas is therefore hotter and less dense in those regions where the debris is most dense; this will be seen to be a significant factor in determining the oxidation rate. Comparison of $\dot{\rho}^4_{O_2}$ with $\dot{\rho}^1_{O_2}$ indicates the effects of the displacement of O_2 due to this thermal expansion of the gas as well as the other effects discussed under 2. and 3. above. Comparison of $\dot{\rho}^4_{O_2}$ with $\dot{\rho}^2_{O_2}$ gives a good indication of the effect of the temperature gradients alone, except near the mouth of the chute.

5.-8. The rates $\dot{\rho}^5_{O_2} - \dot{\rho}^8_{O_2}$, which are rates computed on the basis of O_2 densities identical to $\rho^1_{O_2} - \rho^4_{O_2}$, respectively, but for which the drop-side limits on the reaction rate are ignored. It will be seen that the drop-side limitation affects the values of $\dot{\rho}_{O_2}$.

The code was run with the same input parameters as for the DCH-3 calculation with dripping. The resulting plots of gas temperature, cell-averaged debris temperature, and O_2,N_2^a, and N_2^b mass fractions at $t = 0.58$s are given in Figure 11, and the corresponding eight O_2 consumption rates are given in Figure 12. (Actually the negative of $\dot{\rho}_{O_2}$ is shown, so that the plotted quantities are positive.)

The time of 0.58s occurs just before the end of injection. The debris particle transit time from chute to dome is of the order of 0.1 - 0.2s. Hence, at $t = 0.58$s the injection process has reached a phase reasonably close to a steady state. (Recall that the trapping probability for the dripping case is $p_{trap} = 0.9$, so most of the debris is sticking to the walls. Somewhat less than 10% of it continues to bounce or float around.)

Note also that the narrowness of the injection cone causes the reactions to be very localized near the axis of the container. (The standard deviation of the randomly selected injection angle σ_θ was reduced to 5.7° for the dripping case.) The huge spike in the reaction rates in plots

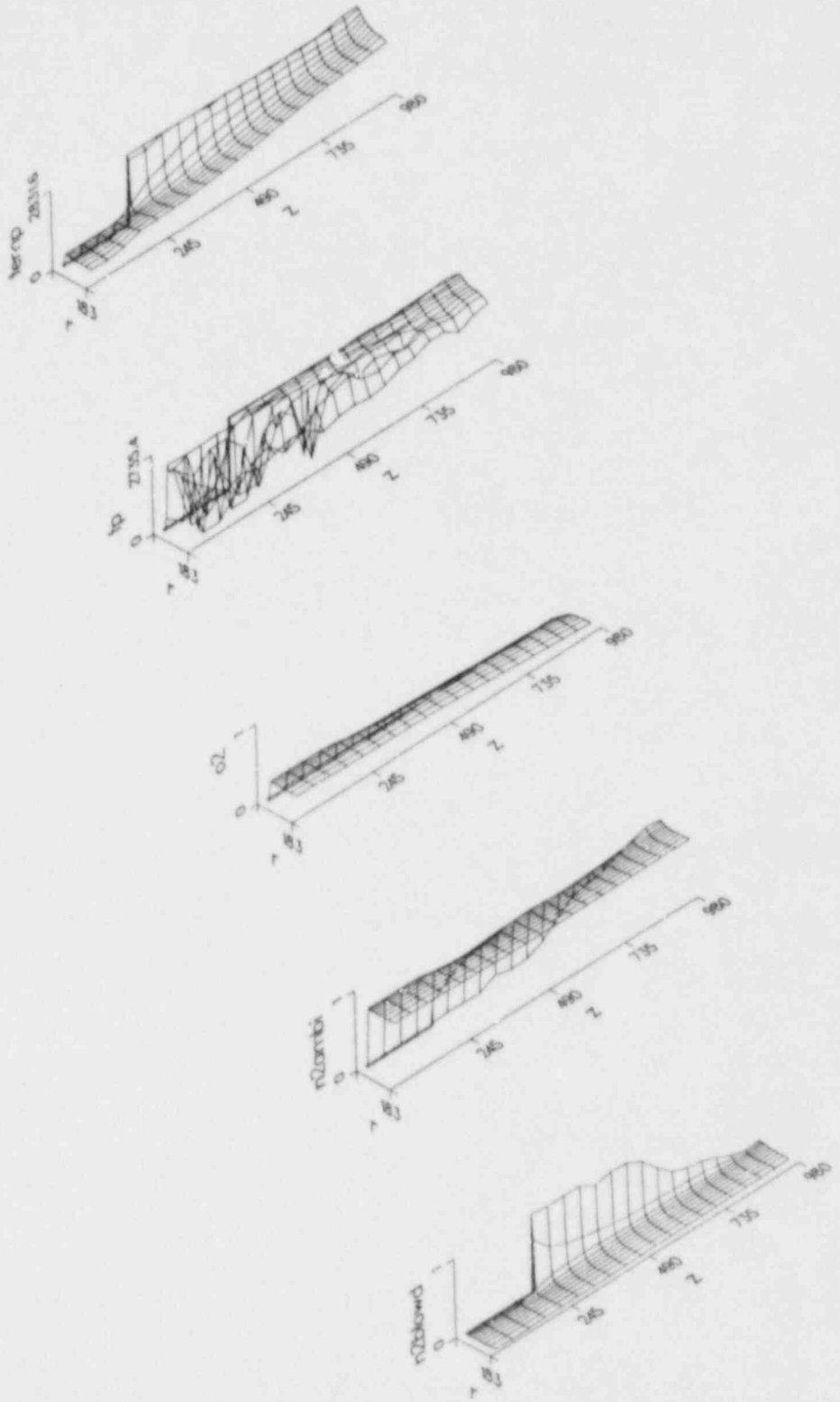

Figure 11. Plots of gas temperature (temp), cell-averaged particle temperature (tp), and mass fractions of oxygen, ambient nitrogen, and blowdown nitrogen (o2, n2ambi, n2blowd) for the DCH-3 simulation at t = 0.58s. Note: The graininess in the particle temperature is due to the somewhat random cell-by-cell existence of computational parcels in some regions.

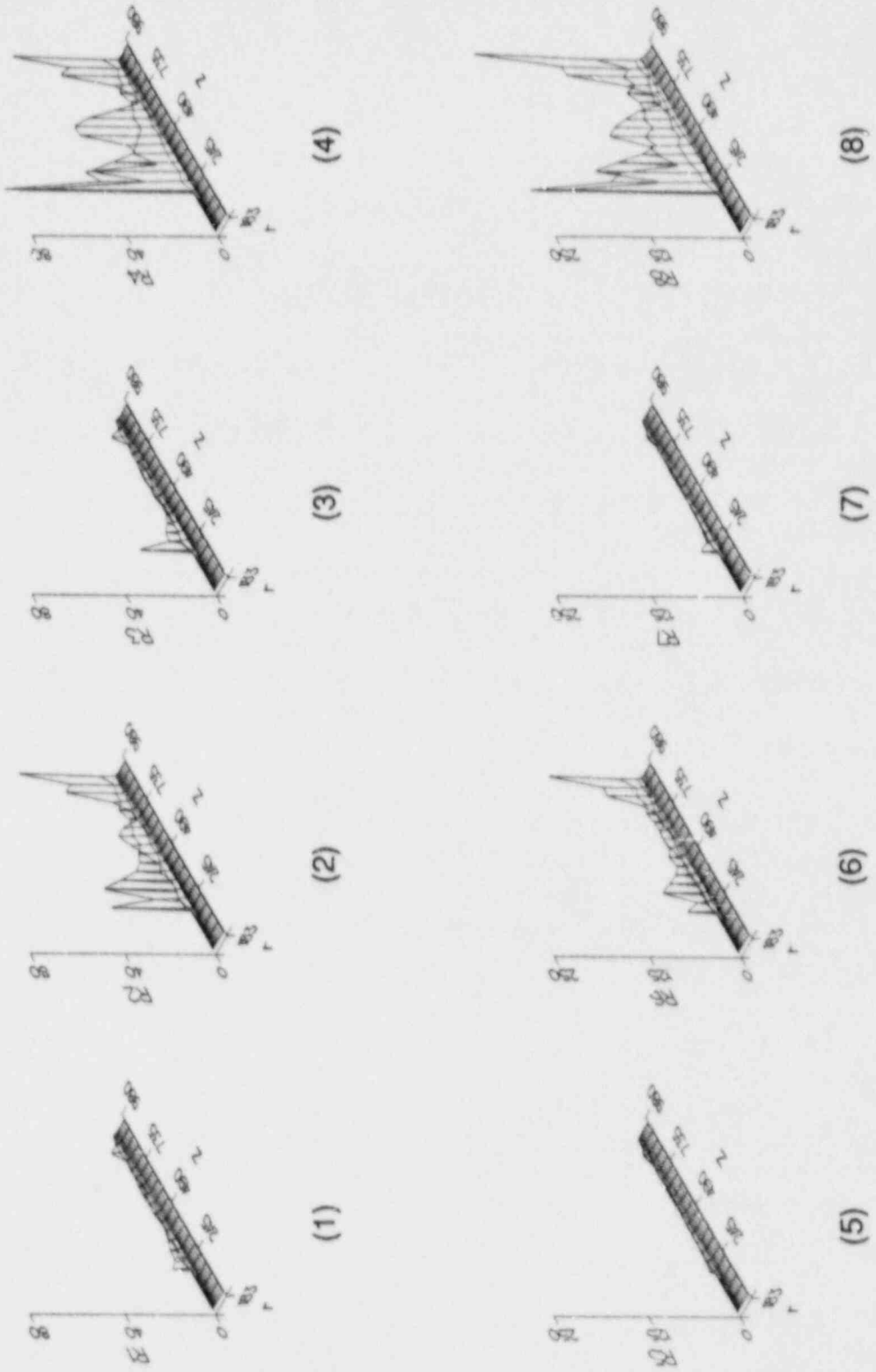

Figure 12. Plots of the rate of oxygen consumption at $t = 0.58$s under various assumptions. Rates are given in kg/(m^3-s) as follows: (1) Rate computed by using the O_2 density actually occurring in the calculation; (2) without oxygen depletion due to reactions; (3) Rate without incursion of driving gas; (4) Rate with initial oxygen concentration (all with drop-side diffusion limits); (5)-(8) Same as (1)-(4), but without drop-side diffusion limits.

(2), (4), (6), and (8) in Figure 12 appears to be due to a random occurrence of several particles in the finite-difference zone there. It doesn't show up in plots (1), (3), (5), and (7) because the oxygen is largely depleted there.

The following points can be inferred from Figure 12:

1. The rate of oxidation is significantly reduced because of the depletion of oxygen by chemical reaction. (Compare plots (1) and (2) on Figure 12.)

2. The displacement of O_2 by the blowdown gas has a significant effect only near the mouth of the chute. (Compare plots (1) and (3).) This is to be expected. Note also that the effect of O_2 depletion by reaction is still larger, even near the chute. (Compare plots (2) and (3).) It is not clear that this should be the case near the mouth of the chute. Future work should determine whether the existence of so much O_2 and ambient gas near the mouth of the chute is due to (a) turbulent diffusion as determined by the eddy viscosity computed from the $k - \epsilon$ model and if so, if the amount is physically plausible, or (b) numerical diffusion caused by the coarse mesh.

3. Displacement of gas due to the temperature gradient is significant. (Compare (1) and (4) or (2) and (4).) It should be emphasized that this can be an important factor in determining the gas-side limitation on the reaction in those situations where thermal mixing has not had time to take place. Note that this effect would be even more pronounced if the drop-side limitation were not important. (Compare (1), (4), and (8).)

4. The drop-side limitation has some effect in the present calculations (compare (1)–(4) with (5)–(8).) Unfortunately, comparison of plots (1) and (5) is difficult on the scale used in Figure 12, while the rates shown in those two plots are the most pertinent, since the actual computed values of ρ_{O_2} are used there. We have found from examination of the computer output that the drop-side limit typically reduces the rates by amounts in the range 0–50%. (I.e., $\dot{\rho}^1_{O_2}$ in plot (1) is smaller than $\dot{\rho}^5_{O_2}$ in plot (5) by such amounts.) The effect of the drop-side limits is much more noticeable in comparing plots (2)–(4) with (6)–(8), because in those cases, the effect of the gas-side limit has generally been reduced by a significant amount.

A Comment on the Computational Results

The above simulations of the experiments with large (80 kg) total debris mass show the trends the data are expected to exhibit in such cases. They have served to emphasize the need for better models for the interaction between the debris and the walls. What are required are *deterministic* methods for describing the sticking of the debris to the surfaces and its subsequent cooling and dripping from the surfaces.

VI. CONCLUSIONS AND FUTURE WORK

This report has described a numerical model for the simulation of the transport of molten debris through a gas. The model includes heat transfer from the debris to the gas and from gas to walls as well as chemical reactions which occur when oxygen in the gas diffuses into the debris particles. The computational methods employed in this work have wide applicability to other combustion problems such as the transport of aerosols and particulates, fire research, spray combustion, and flame acceleration due to obstacle-generated turbulence.[20]

The model has been applied to the simulation of some large-scale experiments relevant to the direct heating of atmospheres in nuclear reactors. It has been shown that good agreement can be obtained between computation and experiment when the total debris mass is so low that the debris particles are significantly cooled by the gas during one transit through the experimental container. As the debris mass is increased, thermal saturation results in nonlinear effects of increasing importance. These effects make accurate simulation strongly dependent on factors which are difficult to model. Of particular importance in this regard is the interaction between the debris and the container walls.

Besides the debris-wall interactions, the studies performed thus far are sensitive to the adequacy of the models for heat transfer and, to a lesser extent, chemical reactions. The sensitivity to accurate treatment of the gas flow in this simple geometric configuration is less acute. This will not be the case in more complex situations with, for example, obstructions placed in the flow. Furthermore, chemical reactions will take on even greater importance when more exothermic reactions are involved. Such reactions anticipated in reactor applications are those involving zirconium and oxygen or steam.

Future work will include improvements in the models for debris-wall interactions and radiative heat transfer. Upcoming experiments with steam will dictate the inclusion of chemical reactions between the metal in the debris and the steam. Finally, we intend to address the important question of the behavior of the debris cloud for geometries in which obstructions appear.

REFERENCES

1. Williams, D. C., Bergeron, K. D., Carroll, D. E., Gasser, R. D., Tills, J. L., and Washington, K. E.: *Containment Loads Due to Direct Containment Heating and Associated Hydrogen Behavior*, Sandia Laboratories Report NUREG/CR-4896, SAND87-0633, 1987.

2. Amsden, A. A., Ramshaw, J. D., O'Rourke, P. J., and Dukowicz, J. K.: *KIVA: A Computer Program for Two- and Three-Dimensional Fluid Flows with Chemical Reactions and Fuel Sprays*, Los Alamos National Laboratory Report LA-10245-MS, 1985.

3. Faeth, G. M.: Prog. Energy Combust. Sci., 9, 1 (1983).

4. Aggarwal, S. K., and Sirignano, W. A.: *Twentieth Symposium (International) on Combustion*, p. 1773, The Combustion Institute, 1985.

5. Beshay, K. R., Gosman, A. D., and Watkins, A. P.: "Assessments of Multidimensional Diesel Spray Predictions," SAE Paper No. 861570 (1986).

6. Tarbell, W. W., Brockman, J. E., Pilch, M., Ross, J. W., Oliver, M. S., Lucero, D. A., Kerley, T. E., Arellano, F. E., and Gomez, R. D.: *Results from the DCH-1 Experiment*, Sandia Report NUREG/CR-4871, SAND86-2483, 1987.

7. Bergeron, K. D., Clauser, M. J., Harrison, B. D., Murata, K. K., Rexroth, P. E., Schelling, F. J., Sciacca, F. W., Senglaub, M. E., Shire, P. R., Trebilcock, W., and Williams, D. C.: *User's Manual for CONTAIN 1.0, a Computer Code for Severe Nuclear Reactor Accident Containment Analysis*, Sandia Laboratories Report NUREG/CR-4085,SAND84-1204 (1985).

8. Jones, W. P.: *Models for Turbulent Flows with Variable Density and Combustion*, in *Prediction Methods for Turbulent Flows*, (W. Kollmann, Ed.), McGraw-Hill, 1980.

9. Rodi, W.: *Turbulence Models and Their Application in Hydraulics*, International Association for Hydraulic Research, Rotterdamseweg 185-P.O. Box 177, 2600 MH Delft, The Netherlands, 1980.

10. Tennekes, H., and Lumley, J. L.(1972): *A First Course in Turbulence*, MIT Press, Massachusetts Institute of Technology, Cambridge, MA.

11. Hinze, J. O.(1975). *Turbulence*, McGraw-Hill, New York.

12. Bird, R. B., Stewart, W. E., and Lightfoot, E. N.: *Transport Phenomena*, Wiley, 1960.

13. Williams, D. C.: Private communication (1987).

14. Siegel, R., and Howell, J. R.: *Thermal Radiation Heat Transfer*, 2nd Ed., Hemisphere, New York, 1981.

15. K. E. Washington, private communication (1987).

16. Raithby, G. D., and Hollands, K. G. T.: *Natural Convection*, in *Handbook of Heat Transfer Fundamentals*, 2nd Ed., (W. M. Rohsenow, J P. Hartnett, and E. N. Ganic, Eds.), McGraw-Hill, 1985.

17. Pilch, M.: Private communication (1987).

18. Tarbell, W. W., Nichols, R. T., Brockman, J. E., Ross, J. W., Oliver, M. S., and Lucero, D. A.: *DCH-2: Results from the Second Experiment Performed in the Surtsey Direct Heating Test Facility*, Sandia Report NUREG/CR-4917, SAND87-0976, 1987.

19. Tarbell, W. W.: Private communication (1987).

20. Marx, K. D., *Development and Application of A Computer Model for Large-Scale Flame Acceleration Experiments*, submitted to Combustion Science and Technology (1987).

UNLIMITED RELEASE

Distribution:

U. S. Government Printing Office
Receiving Branch (Attn: NRC Stock)
8610 Cherry Lane
Laurel, MD 20707
(275 Copies for R4)

U. S. Nuclear Regulatory Commission (23)
Division of Accident Evaluation
Office of Nuclear Regulatory Research
Washington, DC 20555
Attn: E. S. Beckjord
S. B. Burson
L. Chan
M. Cunningham
F. Eltawilla
B. Hardin
L. G. Hulman
C. N. Kelber
T. Lee
R. O. Meyer
G. Marino
J. Mitchell
J. Murphy
C. W. Nilsen
D. F. Ross
Z. Rosztoczy
C. Ryder
M. Silberberg
T. P. Speis
T. Walker
P. Wood
P. Worthington
R. W. Wright

U. S. Nuclear Regulatory Commission (6)
Office of Nuclear Reactor Regulation
Washington, DC 20555
Attn: R. Barrett
J. T. Larkins
S. Long
W. Lyon
R. Palla
C. G. Tinkler

U. S. Department of Energy
R. W. Barber
Office of Nuclear Safety Coordination
Washington, DC 20545

U. S. Department of Energy (2)
Albuquerque Operations Office
Attn. J. R. Roeder, Director
Transportation Safeguards
J. A. Morley, Director
Energy Research Technology
For: C. B. Quinn
R. N. Holton
P.O. Box 5400
Albuquerque, NM 87185

Cathy Anderson
Nuclear Safety Oversight Commission
1133 15th Street, NW
Room 307
Washington DC 20005

D. M. Austin
Office of Energy Research
U. S. Dept. of Energy
ER-7, MS G-226 Germantown
Washington DC 20545

Mr. J. Coleman
Office of Energy Research
U.S. Dept. of Energy
MS G-226 Germantown
Washington, DC 20545

Marvin Gunn, Jr., Manager
Energy Conversion Technology Proj.
Div. of Energy Conversion and
Utilization Technologies C-12
U. S. Department of Energy
1000 Independence Avenue
Washington, D.C. 20585

Ramesh Jain
Buildings and Community Systems
U. S. Department of Energy
1000 Independence Avenue
Washington, D.C. 20585

Dr. A. H. Laufer
Fundamental Interactions Branch
Division of Chemical Sciences
Office of Basic Energy Sciences
U. S. Department of Energy
Washington, D. C. 20545

Dr. Danny C. Lim
Industrial Programs
U. S. Department of Energy
1000 Independence Avenue
Washington, D.C. 20585

Dr. O. Manley
Division of Engineering
and Geosciences
Office of Basic Energy Sciences
Department of Energy
Washington, D.C. 20545

Dr. R. S. Marianelli
Division of Chemical Sciences
U. S. Department of Energy
Washington, D.C. 20585

K. D. Smith, Program Coordinator
Energy Technology Division
DOE Albuquerque Operations Office
Albuquerque, NM 87115

Donald K. Stevens, (Acting)
Associate Director
Basic Energy Sciences
U. S. Department of Energy
Washington, D. C. 20545

Dr. F. Dee Stevenson
Office of Energy Research
U. S. Dept. of Energy
R-142, MS G-226 Germantown
Washington DC 20545

Argonne National Laboratory (6)
Attn: R. Anderson C. Johnson
L. Baker, Jr. J. Rest
Dae Cho B. Spencer
9700 South Cass Avenue
Argonne, IL 60439

Brookhaven National Laboratory (5)
Attn: R. A. Bari T. Pratt
T. Ginsberg N. Tutu
G. Greene
Upton, NY 11973

Los Alamos National Laboratory (7)
Attn: F. J. Edeskuty
R. Gido
J. Carson Mark
G. Schott
M. Stevenson
J. Travis
K. D. Williamson, Jr.
P.O. Box 1663
Los Alamos, NM 87545

A. A. Amsden
T-3, MS-B216
Los Alamos National Laboratory
Los Alamos, NM 87545

T. D. Butler
T-3, MS-B216
Los Alamos National Laboratory
Los Alamos, NM 87544

J. K. Dukowicz
T-3, MS-B216
Los Alamos National Laboratory
Los Alamos, NM 87545

J. Ramshaw
INEL
EG&G Idaho, Inc.
P. O. Box 1625
Idaho Falls, ID 83415

Dr. Elaine Oran
Naval Research Laboratory
Code 4040
Washington, D.C. 20375

Oak Ridge National Laboratory (2)
Attn: A. P. Malinauskas
T. Kress
NRC Programs
P.O. Box X, Bldg. 4500S
Oak Ridge, TN 37831

Prof. Philip J. Smith
Brigham Young University
Department of Chemical Engineering
350 C.B.
Provo, UT 84602

Prof. A. Chorin
Mathematics Department
University of California
Berkeley, CA 94720

Prof. John W. Daily
University of California, Berkeley
Department of Mechanical Engineering
Berkeley, CA 94720

Prof. A. K. Oppenheim
Dept. of Mechanical Engineering
University of California
Berkeley, CA 94720

Robert F. Sawyer
Mechanical Engineering
University of California, Berkeley
Berkeley, CA 94720

Professor R. Seale
Dept. of Nuclear Engineering
University of Arizona
Tucson, AZ 85721

Prof. W. A. Sirignano
Office of the Dean
School of Engineering
University of California, Irvine
Irvine, CA 92717

Prof. W. G. Kollmann
Mechanical Engineering
University of California
Davis, CA 95616

Prof. C. K. Law
Dept. of Mechanical Engineering
University of California
Davis, CA 95616

University of California @ Los Angeles
Nuclear Energy Laboratory (2)
Attn: Prof. I. Catton
Prof. D. Okrent
405 Hilgard Avenue
Los Angeles, CA 90024

Prof. P. Libby
Dept. of Applied Mechanics and
Engineering Science
University of California at
San Diego
La Jolla, CA 92093

Professor S. S. Penner
Energy Center - B-010
University of California,San Diego
La Jolla, CA 92093

Prof. T. G. Theofanous
Chemical and Nuclear Engineerng Dept.
University of California
Santa Barbara, CA 93106

Josette Bellan
Jet Propulsion Laboratory
California Institute Tech.
4800 Oak Grove Drive
Pasadena, CA 91109

Prof. P. E. Dimotakis
Graduate Aeronautical La. 301-46
California Inst. of Technology
Pasadena, CA 91125

A. Leonard
Graduate Aeronautical Lab 301-46
California Inst. of Technology
Pasadena, CA 91125

Prof. K. N. C. Bray
University of Cambridge
Silver St.
Cambridge, CB3 9EW
UNITED KINGDOM

Prof. Norman Chigier
Carnegie-Mellon University
Mechanical Engineering Department
Pittsburgh, PA 15213

Prof. Melvyn C. Branch
University of Colorado
Mechanical Engineering
Boulder, CO 80309

Universita Degli Studi Di Pisa
Attn: M. Carcassi
Dipartmento Di Costruzioni
Meccaniche E. Nucleari
Facolta Di Ingegneria
Via Diotisalvi 2
56100 Pisa
ITALY

Dr. V. P. Roan
College of Engineering
University of Florida
Gainesville, FL 32611

Universität Heidelberg
Attn: Juergen Warnatz
Heidelberg
FEDERAL REPUBLIC OF GERMANY

Professor R. Strehlow
Dept of Aeronautics
University of Illinois
Urbana-Champaign, IL 61801

Imperial College of Science and
Technology
Attn: Dr. A. D. Gosman
Dept. of Mechanical Engineering
Exhibition Road
London SW7 2BX
UNITED KINGDOM

Prof. James H. Whitelaw
Fluids Section
Dept of Mechanical Engineering
Imperial College of Science and Techology
Exhibition Road
London SW7 2BX
UNITED KINGDOM

Dr. A. C. McIntosh
Fuel and Energy Dept.
Leeds University
Leeds LS2 9JT
UNITED KINGLOM

McGill University
Attn: Prof. John H. S. Lee
315 Querbes
Outremont, Quebeck H2V 3W1
CANADA

Simon Engineering Laboratory
Attn: Prof. W. B. Hall
University of Manchester
M139PL
UNITED KINGDOM

Judson R. Baron
Dept. of Aeronautics & Astronautics
Massachusetts Inst. Technology
Room 33-217
Cambridge, MA 02139

Massachusetts Institute of Technology
Attn: N. C. Rasmussen
Nuclear Engineering Department
Cambridge, MA 02139

Claus Borgnakki
Dept. of Mechanical Engineering
University of Michigan
550 East University
Ann Arbor, MI 48109

Dr. G. M. Faeth
University of Michigan
Ann Arbor, MI 48109-2140

University of Michigan
Attn: Prof. M. Sichel
Department of Aerospace Engineering
Ann Arbor, MI 47109

University of Michigan
Nuclear Engineering Department
Ann Arbor, MI 48104

Northwestern University
Attn: Prof. S. G. Bankoff
Chemical Engineering Department
Evanston, IL 60201

Prof. Bernard J. Matkowsky
Dept. of Engineering Sciences
and Applied Mathematics
Northwestern University
Evanston, IL 60201

Prof. Frediano V. Bracco
Princeton University
Department of Mechanical and
Aerospace Engineering
The Engineering Quadrangle
Princeton University
Princeton, NJ 08544

Prof. Forman A. Williams
Dept. of Mechanical and
Aerospace Engineering
Princeton University
Princeton, NJ 08544

Prof. Colin R. Ferguson
Purdue University
Dept. of Mechanical Engineering
North Grant Street
West Lafayette, IN 47907

Rensselaer Polytechnic Institute
Attn: Dr. J. E. Shepherd
Troy, NY 12180-3590

Prof. C. T. Bowman
Stanford University
Mechanical Engineering, Bldg. 520
Stanford, CA 94305

Prof. William Reynolds
Mechanical Engineering Bldg.
Stanford University
Stanford, CA 94305

Institute für Kernenergetik und
Energiesysteme (2)
Attn: M. Buerger
H. Unger
University of Stuttgart
Stuttgart
FEDERAL REPUBLIC OF GERMANY

Prof. R. W. Bilger
Mechanical Engineering
University of Sydney
New South Wales, 2006
Australia

Technische Universität München
Attn: Dr. H. Karwat
8046 Garching
FEDERAL REPUBLIC OF GERMANY

Texas A & M University
Nuclear Engineering Dept.
College Station, TX 77843

UCLA (2)
Nuclear Energy Laboratory
Attn: I. Catton
D. Okrent
405 Hilgaard Avenue
Los Angeles, CA 90024

Prof. J. R. Boven, Dean
College of Engineering
University of Washington
Seattle, WA 98185

Prof. David T. Pratt
University of Washington
Mechanical Engineering FU-10
Seattle, WA 98195

University of Wisconsin
Attn: Prof. M. L. Corradini
Nuclear Engineering Department
1500 Johnson Drive
Madison, WI 53706

Prof. Mitchell D. Smooke
Dept. of Mechanical Engineering
Yale University
New Haven, CT 06520

AERE Harwell
Attn: J. R. Matthews, TPD
Didcot
Oxfordshire OX11 ORA
UNITED KINGDOM

Atomic Energy Ltd.
Attn: H. Rosinger
D. Wren
Whiteshell Nuclear Research
Establishment
Pinawa, Manitoba
CANADA

Atomic Energy Canada Ltd.
Attn: P. Fehrenbach
M. Notley
Chalk River, Ontario KOJ 1J0
CANADA

Battelle Columbus Laboratory (3)
Attn: P. Cybulskis
R. Denning
J Gieseke
505 Kind Avenue
Columbus, OH 43201

Battelle Institut E. V. (3)
Attn: Dr. Werner Geiger
Dr. Guenter Langer
Dr. Manfred Schildknecht
Am Roemerhof 35
6000 Frankfurt am Main 90
FEDERAL REPUBLIC OF GERMANY

Battelle Pacific Northwest Laboratory (2)
Attn: M. Freshley
G. R. Bloom
P.O. Box 999
Richland, WA 99352

Belgonucleaire S. A.
Attn: H. Bairiot
Rue de Champ de Mars 25
B-1050 Brussels
BELGIUM

J. E. Antill
Berkeley Nuclear Laboratory
Berkeley GL 139 PB
Gloucestershire
UNITED KINGDOM

W. G. Cunliffe
Bldg. 396
British Nuclear Fuels, Ltd.
Springfields Work
Salwick, Preston
Lancashire
UNITED KINGDOM

R. Deem
Power Authority State of NY
10 Columbus Circle
New York, NY 10019

Dr. Pierre Joulain
Chimie Phsicque deLa
Combustion ERA160 au CNRS
Domaine du Deffend
Mignaloux Beauvoir
86800 St. Julien l'Ars
FRANCE

Dr. Paul Clavin
Dept. de Combustion
Centre St. Jerome
Marseille Cedex 13 13397
FRANCE

Ktech Corp. (5)
Attn: R. E. Blose M. S. Oliver
J. Jackson J. W. Ross
R. T. Nichols
901 Pennsylvania NE
Albuquerque, NM 87110

Paul Thibault
Combustion Dynamics Ltd.
Box 175
Ralston, Alberta
Canada T0J 2N0

Dr. Rudy Maly
Daimler Benz AG
Abteilung E6T/E
Postfach 202
D-7000 Stuttgart
West Germany

John H. Pohl
Energy & Environmental Research Corp.
18 Mason
Irvine, CA 92718

Electric Power Research Institute (4)
Attn: W. Loewenstein
R. Ritzman
B. R. Sehgal
R. Vogel
3412 Hillview Avenue
Palo Alto, CA 94303

Nucleare e della Protezione
Sanitaria (DISP)(2)
Attn: Mr. Manilia
Mr. G. Petrangeli
Ente Nazionnle Energie
Alternatie (ENEA)
Viale Regina Margherita, 125
Casella Postale M. 2358
I-00100 Roma A. D., ITALY

Factory Mutual Research Corporation
Attn: R. Zalosh
P.O. Box 688
Norwood, MA 02062

Fauske & Associates (2)
Attn: R. Henry
M. Plys
16W070 West 83rd Street
Burr Ridge, IL 60521

Rolf D. Reitz
Fluid Mechanics Dept.
General Motors
GM Technical Center
Warren, MI 48090

James A. Kezerle
Gas Research Institute
8600 West Bryn Mawr Ave
Chicago, Il 60631

General Electric Corporation
Attn: K. W. Holtzclaw
175 Curtner Avenue
Mail Code N 1C157
San Jose, CA 95125

General Electric Corporation
Attn: M. I. Temme, Manager
Probabilistic Risk Assessment
Advanced Reactor Systems Dept.
P.O. Box 3508
Sunnyvale, CA 94088

Charles A. Ahmann
G. M. Research Laboratories
Twelve Mile and Mound Roads
P. O. Box 9055
Warren, MI 48090-9055

Dr. Roger B. Krieger
G. M. Research Laboratories
Twelve Mile and Mound Roads
P. O. Box 9055
Warren, MI 48090-9055

Gesellschaft fur Reaktorsicherheit (GRS)
Postfach 101650
Glockengasse 2
5000 Köln 1
FEDERAL REPUBLIC OF GERMANY

Gesellschaft für Reaktorsicherheit (2)
Attn: Dr. E. F. Hicken
Dr. H. L. Jahn
8046 Garching
Forschungsgelande
FEDERAL REPUBLIC OF GERMANY

International Technology Corporation
Attn: Mario H. Fontana
575 Oak Ridge Turnpike
Oak Ridge, TN 37830

Japan Atomic Energy Research Institute (2)
Attn: Dr. K. Soda, Manager
S. Saito
Chemical Engineering Safety Laboratory
Dept. of Nuclear Fuel Safety
Tokai-mura, Naku-gun Ibaraki-ken
319-11
JAPAN

Japan Atomic Energy Research Institute
Attn: Dr. T. Fujishiro, Manager
Dept. of Fuel Safety Research
Tokai-mura, Naka-gun, Ibaraki-ken
319-11
JAPAN

Japan Atomic Energy Research Institute
Attn: Dr. Kazuo Sato, Director
Dept. of Reactor Safety Research
Tokai-mura, Naka-gun Ibaraki-ken
319-11
JAPAN

Kraftwerk Union
Attn: Dr. M. Peehs
Hammerbacherstrasse 12 & 14
Postfach 3220
D-8520 Erlangen 2
FEDERAL REPUBLIC OF GERMANY

Lehrgebiet für Mechanik der
RWTH Aachen
Attn: Prof. Dr. Ing. N. Peters
Templergraben 55
D5100 Aachen
FEDERAL REPUBLIC OF GERMANY

Wang Lu
TVA
400 Commerce, W9C157-CK
Knoxville, TN 37902

Dr. Ingar O. Moen
Head/Shock and Blast Group
Defence Research Establishment
Suffield
Ralston, Alberta
CANADA TOJ 2NO

Netherlands Energy Research Foundation
Attn: K. J. Brinkmann
P.O. Box 1
1755ZG Petten NH
NETHERLANDS

Risk Management Associates
Peter Bieniarz
2309 Dietz Farm Road, NW
Albuquerque, NM 87107

M. Jankovski
IAEA
Division of Nuclear Reactor Safety
Wagranerstrasse 5
P. O. Box 100
A/1400 Vienna
AUSTRIA

R. Sherry
JAYCOR
P. O. Box 85154
San Diego, CA 92138

Dr. Arthur A. Boni
Physical Sciences Inc.
P. O. Box 3100
Andover, MA 01810

Kernforschungszentrum Karlsruhe
Attn: H. Rininsland
Postfach 3640
75 Karsruhe
FEDERAL REPUBLIC OF GERMANY

Pak-Yan Liang
Rockwell Int'l, Rocketdyne Div.
6633 Canoga Ave., FB47
Canoga Park, CA 91303

C. H. Priddin
Mgr. Combustion Methods
Rolls-Royce plc
P. O. Box 31
Derby DE28BJ
UNITED KINGDOM

Shell Research Ltd.
Paul H. Taylor
Thornton Research Centre
P.O. Box 1
Chester CH1 3SH
UNITED KINGDOM

Jana Backovsky
SRI International
33 Ravenswood Avenue
Menlo Park, CA 94025

Stratton & Associates, Inc.
Attn: W. Stratton
2 Acoma Lane
Los Alamos, NM 87544

Statens Karnkraftinspektion
Attn: L. Hammar
P.O. Box 27106
S-10252 Stockholm
SWEDEN

Studsvik Energiteknik AB
Attn: K. Johansson
S-611 82 Nykoping
SWEDEN

Swedish State Power Board
Attn: Wiktor Frid
S-162 Fach 87 Vallingby
SWEDEN

UKAEA Safety & Reliability
Directorate (3)
Attn: J. H. Gittus
M. R. Hayns
H. J. Teague
Wigshaw Lane, Culcheth
Warrington WA3 4NE
Cheshire
UNITED KINGDOM

UKAEA, Culham Laboratory
Attn: F. Briscoe
Abingdon
Oxfordshire OX14 3DB
UNITED KINGDOM

UKAEA AEE Winfrith (6)
Attn: B. Bowsher R. Potter
T. Butland P. Smith
A. Nichols S. Kinnersley
Dorchester
Dorset DT2 8DH
UNITED KINGDOM

Dr. S. J. Niemczyk
1545 18th Street, NW
#112
Washington DC 20036

L. Cloutman, L-035
Lawrence Livermore National Lab.
Livermore, CA 94550

C. K. Westbrook, L-321
Lawrence Livermore National Lab.
Livermore, CA 94550

1131 W. B. Benedick
1510 J. W. Nunziato
1512 J. C. Cummings
1513 M. R. Baer
1636 F. G. Blottner
6400 D. J. McCloskey
6412 A. L. Camp
6420 J. V. Walker
6422 D. A. Powers
6422 W. W. Tarbell

6425 W. J. Camp
6425 M. Pilch
6425 M. F. Young
6427 M. Berman
6427 L. S. Nelson
6427 M. P. Sherman
6427 S. R. Tieszen
6429 K. D. Bergeron
6429 D. E. Carroll
6429 K. E. Washington
6429 D. C. Williams
6440 D. A. Dahlgren
8000 J. C. Crawford
8100 E. E. Ives
8200 R. J. Detry
8240 C. W. Robinson
Attn: 8244 C. M. Hartwig
8245 R. J. Kee
8245 A. E. Lutz
8244 D. R. Chenoweth
8245 S. Paolucci
8300 P. L. Mattern
Attn 8310 R. W. Rohde
8340 W. Bauer
8350 J. S. Binkley
Attn: 8351 J. Y. Chen
8351 R. P. Lucht
8353 G. A. Fisk
8354 R. E. Palmer
8357 R. J. Carling
8360 W. J. McLean
8361 D. R. Hardesty
Attn: 8361 T. Fletcher
8362 T. M. Dyer
Attn: 8362 C. F. Edwards
8362 D. L. Siebers

8363 B. R. Sanders
Attn: 8363 W. T. Ashurst
8363 P. K. Barr
8363 H. A. Dwyer
8363 A. R. Kerstein
8363 S. B. Margolis
8363 K. D. Marx (5)
8364 S. C. Johnston
8400 R. C. Wayne
8500 P. E. Brewer
8535 Publication Division/
Tech. Library Proc. Div. 3141
8524 P. W. Dean,
Central Technical Files (3)
3141 Tech. Library Proc. Div. (3)
3151 W. L. Garner

120555137330 1 1AN1R4
US NRC-OARM-ADM
DIV FOIA & PUBLICATIONS SVCS
SECTION CHIEF
REGULATORY PUBLICATION SECT
P-210
WASHINGTON DC 20555

Org.	Bldg.	Name	Rec'd by	Org.	Bldg.	Name	Rec'd by

Sandia National Laboratories